Combining the AFLOW GIBBS and elastic libraries to efficiently and robustly screen thermomechanical properties of solids

Cormac Toher,[1] Corey Oses,[1] Jose J. Plata,[1] David Hicks,[1] Frisco Rose,[1] Ohad Levy,[1,2] Maarten de Jong,[3,4] Mark Asta,[3] Marco Fornari,[5] Marco Buongiorno Nardelli,[6] and Stefano Curtarolo[7,*]

[1]*Department of Mechanical Engineering and Materials Science, Duke University, Durham, North Carolina 27708, USA*
[2]*Department of Physics, NRCN, Beer-Sheva, 84190, Israel*
[3]*Department of Materials Science and Engineering, University of California, Berkeley, 210 Hearst Memorial Mining Building, Berkeley, California 94720, USA*
[4]*Space Exploration Technologies, 1 Rocket Road, Hawthorne, California 90250, USA*
[5]*Department of Physics, Central Michigan University, Mount Pleasant, Michigan 48858, USA*
[6]*Department of Physics and Department of Chemistry, University of North Texas, Denton, Texas 76203, USA*
[7]*Materials Science, Electrical Engineering, Physics and Chemistry, Duke University, Durham, North Carolina 27708, USA*

(Received 8 September 2016; published 19 June 2017)

Thorough characterization of the thermomechanical properties of materials requires difficult and time-consuming experiments. This severely limits the availability of data and is one of the main obstacles for the development of effective accelerated materials design strategies. The rapid screening of new potential materials requires highly integrated, sophisticated, and robust computational approaches. We tackled the challenge by developing an automated, integrated workflow with robust error-correction within the AFLOW framework which combines the newly developed "Automatic Elasticity Library" with the previously implemented GIBBS method. The first extracts the mechanical properties from automatic self-consistent stress-strain calculations, while the latter employs those mechanical properties to evaluate the thermodynamics within the Debye model. This new thermoelastic workflow is benchmarked against a set of 74 experimentally characterized systems to pinpoint a robust computational methodology for the evaluation of bulk and shear moduli, Poisson ratios, Debye temperatures, Grüneisen parameters, and thermal conductivities of a wide variety of materials. The effect of different choices of equations of state and exchange-correlation functionals is examined and the optimum combination of properties for the Leibfried-Schlömann prediction of thermal conductivity is identified, leading to improved agreement with experimental results than the GIBBS-only approach. The framework has been applied to the AFLOW.org data repositories to compute the thermoelastic properties of over 3500 unique materials. The results are now available online by using an expanded version of the REST-API described in the Appendix.

DOI: 10.1103/PhysRevMaterials.1.015401

I. INTRODUCTION

Calculating the thermal and elastic properties of materials is important for predicting the thermodynamic and mechanical stability of structural phases [1–4] and assessing their importance for a variety of applications. Elastic and mechanical properties such as the shear and bulk moduli are important for predicting the hardness of materials [5], and thus their resistance to wear and distortion. Thermal properties, such as specific heat capacity and lattice thermal conductivity, are important for applications including thermal barrier coatings, thermoelectrics [6–8], and heat sinks [9,10].

Elasticity. There are two main methods for calculating the elastic constants, based on the response of either the stress tensor or the total energy to a set of applied strains [11–16]. In this study, we obtain the elastic constants from the calculated stress tensors for a set of independent deformations of the crystal lattice. This method is implemented within the AFLOW framework for computational materials design [17–19], where it is referred to as the Automatic Elasticity Library (AEL). A similar implementation within the Materials Project [14] allows extensive screening studies by combining data from these two large repositories of computational materials data.

Thermal properties. The determination of the thermal conductivity of materials from first principles requires either calculation of anharmonic interatomic force constants (IFCs) for use in the Boltzmann transport equation (BTE) [20–27], or molecular dynamics simulations in combination with the Green-Kubo formula [28,29], both of which are highly demanding computationally even within multiscale approaches [30]. These methods are unsuitable for rapid generation and screening of large databases of materials properties in order to identify trends and simple descriptors [31]. Previously, we have implemented the "GIBBS" quasiharmonic Debye model [32,33] within both the Automatic GIBBS Library (AGL) [34] of the AFLOW [17,35–38], and Materials Project [39–41] frameworks. This approach does not require large supercell calculations since it relies merely on first-principles calculations of the energy as a function of unit cell volume. It is thus much more tractable computationally and eminently suited to investigating the thermal properties of entire classes of materials in a highly automated fashion to identify promising candidates for more in-depth experimental and computational analysis.

The data set of computed thermal and elastic properties produced for this study is available in the AFLOW [35] online data repository, either using the AFLOW representational state transfer application programming interface (REST-API) [36] or via the aflow.org web portal [35,42].

*stefano@duke.edu

II. THE AEL-AGL METHODOLOGY

The AEL-AGL methodology combines elastic constants calculations, in the Automatic Elasticity Library (AEL), with the calculation of thermal properties within the Automatic GIBBS Library (AGL [34])—"GIBBS" [32] implementation of the Debye model. This integrated software library includes automatic error correction to facilitate high-throughput computation of thermal and elastic materials properties within the AFLOW framework [17,35–37,43–47]. The principal ingredients of the calculation are described in the following sections.

A. Elastic properties

The elastic constants are evaluated from the stress-strain relations

$$\begin{pmatrix} s_{11} \\ s_{22} \\ s_{33} \\ s_{23} \\ s_{13} \\ s_{12} \end{pmatrix} = \begin{pmatrix} c_{11} & c_{12} & c_{13} & c_{14} & c_{15} & c_{16} \\ c_{12} & c_{22} & c_{23} & c_{24} & c_{25} & c_{26} \\ c_{13} & c_{23} & c_{33} & c_{34} & c_{35} & c_{36} \\ c_{14} & c_{24} & c_{34} & c_{44} & c_{45} & c_{46} \\ c_{15} & c_{25} & c_{35} & c_{45} & c_{55} & c_{56} \\ c_{16} & c_{26} & c_{36} & c_{46} & c_{56} & c_{66} \end{pmatrix} \begin{pmatrix} \epsilon_{11} \\ \epsilon_{22} \\ \epsilon_{33} \\ 2\epsilon_{23} \\ 2\epsilon_{13} \\ 2\epsilon_{12} \end{pmatrix} \quad (1)$$

with stress tensor elements s_{ij} calculated for a set of independent normal and shear strains ϵ_{ij}. The elements of the elastic stiffness tensor c_{ij}, written in the 6×6 Voigt notation using the mapping [2] $11 \mapsto 1, 22 \mapsto 2, 33 \mapsto 3, 23 \mapsto 4, 13 \mapsto 5, 12 \mapsto 6$, are derived from polynomial fits for each independent strain, where the polynomial degree is automatically set to be less than the number of strains applied in each independent direction to avoid overfitting. The elastic constants are then used to compute the bulk and shear moduli, using either the Voigt approximation

$$B_{\text{Voigt}} = \tfrac{1}{9}[(c_{11} + c_{22} + c_{33}) + 2(c_{12} + c_{23} + c_{13})] \quad (2)$$

for the bulk modulus, and

$$G_{\text{Voigt}} = \tfrac{1}{15}[(c_{11} + c_{22} + c_{33}) - (c_{12} + c_{23} + c_{13})] + \tfrac{1}{5}(c_{44} + c_{55} + c_{66}) \quad (3)$$

for the shear modulus, or the Reuss approximation, which uses the elements of the compliance tensor s_{ij} (the inverse of the stiffness tensor), where the bulk modulus is given by

$$\frac{1}{B_{\text{Reuss}}} = (s_{11} + s_{22} + s_{33}) + 2(s_{12} + s_{23} + s_{13}) \quad (4)$$

and the shear modulus is

$$\frac{15}{G_{\text{Reuss}}} = 4(s_{11} + s_{22} + s_{33}) - 4(s_{12} + s_{23} + s_{13}) + 3(s_{44} + s_{55} + s_{66}). \quad (5)$$

For polycrystalline materials, the Voigt approximation corresponds to assuming that the strain is uniform and that the stress is supported by the individual grains in parallel, giving the upper bound on the elastic moduli, while the Reuss approximation assumes that the stress is uniform and that the strain is the sum of the strains of the individual grains in series, giving the lower bound on the elastic moduli [2]. The two approximations can be combined in the Voigt-Reuss-Hill (VRH) [48] averages for the bulk modulus,

$$B_{\text{VRH}} = \frac{B_{\text{Voigt}} + B_{\text{Reuss}}}{2}, \quad (6)$$

and the shear modulus,

$$G_{\text{VRH}} = \frac{G_{\text{Voigt}} + G_{\text{Reuss}}}{2}. \quad (7)$$

The Poisson ratio σ is then obtained by

$$\sigma = \frac{3B_{\text{VRH}} - 2G_{\text{VRH}}}{6B_{\text{VRH}} + 2G_{\text{VRH}}}. \quad (8)$$

These elastic moduli can also be used to compute the speed of sound for the transverse and longitudinal waves, as well as the average speed of sound in the material [2]. The speed of sound for the longitudinal waves is

$$v_{\text{L}} = \left(\frac{B + \frac{4}{3}G}{\rho}\right)^{\frac{1}{2}}, \quad (9)$$

and for the transverse waves

$$v_{\text{T}} = \left(\frac{G}{\rho}\right)^{\frac{1}{2}}, \quad (10)$$

where ρ is the mass density of the material. The average speed of sound is then evaluated by

$$\overline{v} = \left[\frac{1}{3}\left(\frac{2}{v_{\text{T}}^3} + \frac{1}{v_{\text{L}}^3}\right)\right]^{-\frac{1}{3}}. \quad (11)$$

B. The AGL quasiharmonic Debye-Grüneisen model

The Debye temperature of a solid can be written as [2]

$$\theta_{\text{D}} = \frac{\hbar}{k_{\text{B}}}\left(\frac{6\pi^2 n}{V}\right)^{1/3}\overline{v}, \quad (12)$$

where n is the number of atoms in the cell, V is its volume, and $\overline{v}$ is the average speed of sound of Eq. (11). It can be shown by combining Eqs. (8)–(11) that $\overline{v}$ is equivalent to [2]

$$\overline{v} = \sqrt{\frac{B_{\text{S}}}{\rho}}\, f(\sigma), \quad (13)$$

where B_{S} is the adiabatic bulk modulus, ρ is the density, and $f(\sigma)$ is a function of the Poisson ratio σ:

$$f(\sigma) = \left\{3\left[2\left(\frac{2}{3} \times \frac{1+\sigma}{1-2\sigma}\right)^{3/2} + \left(\frac{1}{3} \times \frac{1+\sigma}{1-\sigma}\right)^{3/2}\right]^{-1}\right\}^{\frac{1}{3}}. \quad (14)$$

In an earlier version of AGL [34], the Poisson ratio in Eq. (14) was assumed to have the constant value $\sigma = 0.25$, which is the ratio for a Cauchy solid. This was found to be a reasonable approximation, producing good correlations with experiment. The AEL approach, Eq. (8), directly evaluates σ assuming only

that it is independent of temperature and pressure. Substituting Eq. (13) into Eq. (12), the Debye temperature is obtained as

$$\theta_D = \frac{\hbar}{k_B}[6\pi^2 V^{1/2} n]^{1/3} f(\sigma)\sqrt{\frac{B_S}{M}}, \tag{15}$$

where M is the mass of the unit cell. The bulk modulus B_S is obtained from a set of DFT calculations for different volume cells, either by fitting the resulting $E_{DFT}(V)$ data to a phenomenological equation of state or by taking the numerical second derivative of a polynomial fit:

$$\begin{aligned} B_S(V) &\approx B_{static}(\vec{x}) \approx B_{static}(\vec{x}_{opt}(V)) \\ &= V\left(\frac{\partial^2 E(\vec{x}_{opt}(V))}{\partial V^2}\right) = V\left(\frac{\partial^2 E(V)}{\partial V^2}\right). \end{aligned} \tag{16}$$

Inserting Eq. (16) into Eq. (15) gives the Debye temperature as a function of volume $\theta_D(V)$, for each value of pressure p and temperature T.

The equilibrium volume at any particular (p,T) point is obtained by minimizing the Gibbs free energy with respect to volume. First, the vibrational Helmholtz free energy, $F_{vib}(\vec{x};T)$, is calculated in the quasiharmonic approximation

$$F_{vib}(\vec{x};T) = \int_0^\infty \left[\frac{\hbar\omega}{2} + k_B T \ \ln(1 - e^{-\hbar\omega/k_B T})\right] g(\vec{x};\omega) d\omega, \tag{17}$$

where $g(\vec{x};\omega)$ is the phonon density of states and $\vec{x}$ describes the geometrical configuration of the system. In the Debye-Grüneisen model, F_{vib} can be expressed in terms of the Debye temperature θ_D,

$$F_{vib}(\theta_D;T) = nk_B T\left[\frac{9}{8}\frac{\theta_D}{T} + 3 \ \ln(1 - e^{-\theta_D/T}) - D\left(\frac{\theta_D}{T}\right)\right], \tag{18}$$

where $D(\theta_D/T)$ is the Debye integral

$$D(\theta_D/T) = 3\left(\frac{T}{\theta_D}\right)^3 \int_0^{\theta_D/T} \frac{x^3}{e^x - 1} dx. \tag{19}$$

The Gibbs free energy is calculated as

$$\mathsf{G}(V;p,T) = E_{DFT}(V) + F_{vib}(\theta_D(V);T) + pV, \tag{20}$$

and fitted by a polynomial of V. The equilibrium volume, V_{eq}, is that which minimizes $\mathsf{G}(V;p,T)$. Once V_{eq} has been determined, θ_D can be determined, and then other thermal properties including the Grüneisen parameter and thermal conductivity can be calculated as described in the following sections.

C. Equations of state

Within AGL, the bulk modulus can be determined either numerically from the second derivative of the polynomial fit of $E_{DFT}(V)$, Eq. (16), or by fitting the (p,V) data to a phenomenological equation of state (EOS). Three different analytic EOS have been implemented within AGL: the Birch-Murnaghan EOS [2,32,49], the Vinet EOS [32,50], and the Baonza-Cáceres-Núñez spinodal EOS [32,51].

The Birch-Murnaghan EOS is

$$\frac{p}{3f(1+2f)^{\frac{5}{2}}} = \sum_{i=0}^{2} a_i f^i, \tag{21}$$

where p is the pressure, a_i are polynomial coefficients, and f is the "compression" given by

$$f = \frac{1}{2}\left[\left(\frac{V}{V_0}\right)^{-\frac{2}{3}} - 1\right]. \tag{22}$$

The zero pressure bulk modulus is equal to the coefficient a_0.

The Vinet EOS is [32,50]

$$\ln\left[\frac{px^2}{3(1-x)}\right] = \ln B_0 + a(1-x), \tag{23}$$

where a and $\ln B_0$ are fitting parameters and

$$x = \left(\frac{V}{V_0}\right)^{\frac{1}{3}}, \quad a = 3(B_0' - 1)/2. \tag{24}$$

The isothermal bulk modulus B_T is given by [32,50]

$$B_T = -x^{-2} B_0 e^{a(1-x)} f(x), \tag{25}$$

where

$$f(x) = x - 2 - ax(1-x).$$

The Baonza-Cáceres-Núñez spinodal equation of state has the form [32,51]

$$V = V_{sp} \exp\left[-\left(\frac{K^*}{1-\beta}\right)(p - p_{sp})^{1-\beta}\right], \tag{26}$$

where K^*, p_{sp}, and β are the fitting parameters, and V_{sp} is given by

$$V_{sp} = V_0 \exp\left[\frac{\beta}{(1-\beta)B_0'}\right],$$

where $B_0 = [K^*]^{-1}(-p_{sp})^\beta$ and $B_0' = (-p_{sp})^{-1}\beta B_0$. The isothermal bulk modulus B_T is then given by [32,51]

$$B_T = \frac{(p - p_{sp})^\beta}{K^*}. \tag{27}$$

Note that AGL uses B_T instead of B_S in Eq. (15) when one of these phenomenological EOS is selected. B_S can then be calculated as

$$B_S = B_T(1 + \alpha\gamma T), \tag{28}$$

where γ is the Grüneisen parameter (described in Sec. II D below), and α is the thermal expansion

$$\alpha = \frac{\gamma C_V}{B_T V}, \tag{29}$$

where C_V is the heat capacity at constant volume, given by

$$C_V = 3nk_B\left[4D\left(\frac{\theta_D}{T}\right) - \frac{3\theta_D/T}{\exp(\theta_D/T) - 1}\right]. \tag{30}$$

D. The Grüneisen parameter

The Grüneisen parameter describes the variation of the thermal properties of a material with the unit cell size and contains information about higher order phonon scattering, which is important for calculating the lattice thermal conductivity [34,52–55] and thermal expansion [2,32,56]. It is defined as the phonon frequencies dependence on the unit cell volume:

$$\gamma_i = -\frac{V}{\omega_i}\frac{\partial \omega_i}{\partial V}. \tag{31}$$

Debye's theory assumes that the volume dependence of all mode frequencies is the same as that of the cutoff Debye frequency, so the Grüneisen parameter can be expressed in terms of θ_D:

$$\gamma = -\frac{\partial \ \ln(\theta_D(V))}{\partial \ \ln V}. \tag{32}$$

This macroscopic definition of the Debye temperature is a weighted average of Eq. (31) with the heat capacities for each branch of the phonon spectrum:

$$\gamma = \frac{\sum_i \gamma_i C_{V,i}}{\sum_i C_{V,i}}. \tag{33}$$

Within AGL [34], the Grüneisen parameter can be calculated in several different ways, including direct evaluation of Eq. (32), by using the more stable Mie-Grüneisen equation [2],

$$p - p_{T=0} = \gamma \frac{U_{\text{vib}}}{V}, \tag{34}$$

where U_{vib} is the vibrational internal energy [32]

$$U_{\text{vib}} = nk_B T\left[\frac{9}{8}\frac{\theta_D}{T} + 3D\left(\frac{\theta_D}{T}\right)\right]. \tag{35}$$

The "Slater gamma" expression [2]

$$\gamma = -\frac{1}{6} + \frac{1}{2}\frac{\partial B_S}{\partial p} \tag{36}$$

is the default method in the automated workflow used for the AFLOW database.

E. Thermal conductivity

In the AGL framework, the thermal conductivity is calculated using the Leibfried-Schlömann equation [52–54]

$$\kappa_l(\theta_a) = \frac{0.849 \times 3\sqrt[3]{4}}{20\pi^3\left(1-0.514\gamma_a^{-1}+0.228\gamma_a^{-2}\right)}\left(\frac{k_B\theta_a}{\hbar}\right)^2\frac{k_B m V^{\frac{1}{3}}}{\hbar\gamma_a^2}, \tag{37}$$

where V is the volume of the unit cell and m is the average atomic mass. It should be noted that the Debye temperature and Grüneisen parameter in this formula, θ_a and γ_a, are slightly different from the traditional Debye temperature, θ_D, calculated in Eq. (15) and Grüneisen parameter, γ, obtained from Eq. (36). Instead, θ_a and γ_a are obtained by only considering the acoustic modes, based on the assumption that the optical phonon modes in crystals do not contribute to heat transport [53]. This θ_a is referred to as the "acoustic" Debye temperature [53,54]. It can be derived directly from the phonon DOS by integrating only over the acoustic modes [53,57]. Alternatively, it can be calculated from the traditional Debye temperature θ_D [53,54]:

$$\theta_a = \theta_D n^{-\frac{1}{3}}. \tag{38}$$

There is no simple way to extract the "acoustic" Grüneisen parameter from the traditional Grüneisen parameter. Instead, it must be calculated from Eq. (31) for each phonon branch separately and summed over the acoustic branches [56,58]. This requires using the quasiharmonic phonon approximation, which involves calculating the full phonon spectrum for different volumes [56–58], and is therefore too computationally demanding to be used for high-throughput screening, particularly for large, low-symmetry systems. Therefore we use the approximation $\gamma_a = \gamma$ in the AEL-AGL approach to calculate the thermal conductivity. The dependence of the expression in Eq. (37) on γ is weak [34,54], thus the evaluation of κ_l using the traditional Grüneisen parameter introduces just a small systematic error, which is insignificant for screening purposes [58].

The thermal conductivity at temperatures other than θ_a is estimated by [53–55]

$$\kappa_l(T) = \kappa_l(\theta_a)\frac{\theta_a}{T}. \tag{39}$$

F. DFT calculations and workflow details

The DFT calculations to obtain $E(V)$ and the strain tensors were performed using the VASP software [59] with projector-augmented-wave pseudopotentials [60] and the PBE parametrization of the generalized gradient approximation to the exchange-correlation functional [61], using the parameters described in the AFLOW Standard [37]. The energies were calculated at zero temperature and pressure, with spin polarization and without zero-point motion or lattice vibrations. The initial crystal structures were fully relaxed (cell volume and shape and the basis atom coordinates inside the cell).

For the AEL calculations, four strains were applied in each independent lattice direction (two compressive and two expansive) with a maximum strain of 1% in each direction, for a total of 24 configurations [14]. For cubic systems, the crystal symmetry was used to reduce the number of required strain configurations to eight. For each configuration, two ionic positions AFLOW Standard RELAX [37] calculations at fixed cell volume and shape were followed by a single AFLOW Standard STATIC [37] calculation. The elastic constants are then calculated by fitting the elements of stress tensor obtained for each independent strain. The stress tensor from the zero-strain configuration (i.e., the initial unstrained relaxed structure) can also be included in the set of fitted strains, although this was found to have negligible effect on the results. Once these calculations are complete, it is verified that the eigenvalues of the stiffness tensor are all positive, that the stiffness tensor obeys the appropriate symmetry rules for the lattice type [3], and that the applied strain is still within the linear regime, using the method described by de Jong *et al.* [14]. If any of these conditions fail, the calculation is repeated with adjusted applied strain.

The AGL calculation of $E(V)$ is fitted to the energy at 28 different volumes of the unit cell obtained by increasing or decreasing the relaxed lattice parameters in fractional

increments of 0.01, with a single AFLOW Standard STATIC [37] calculation at each volume. The resulting $E(V)$ data are checked for convexity and to verify that the minimum energy is at the initial volume (i.e., at the properly relaxed cell size). If any of these conditions fail, the calculation is repeated with adjusted parameters, e.g., increased k-point grid density.

G. Correlation analysis

Pearson and Spearman correlations are used to analyze the results for entire sets of materials. The Pearson coefficient r is a measure of the linear correlation between two variables, X and Y. It is calculated by

$$r = \frac{\sum_{i=1}^{n}(X_i - \overline{X})(Y_i - \overline{Y})}{\sqrt{\sum_{i=1}^{n}(X_i - \overline{X})^2}\sqrt{\sum_{i=1}^{n}(Y_i - \overline{Y})^2}}, \tag{40}$$

where $\overline{X}$ and $\overline{Y}$ are the mean values of X and Y.

The Spearman coefficient ρ is a measure of the monotonicity of the relation between two variables. The raw values of the two variables X_i and Y_i are sorted in ascending order, and are assigned rank values x_i and y_i which are equal to their position in the sorted list. If there is more than one variable with the same value, the average of the position values is assigned to all duplicate entries. The correlation coefficient is then given by

$$\rho = \frac{\sum_{i=1}^{n}(x_i - \overline{x})(y_i - \overline{y})}{\sqrt{\sum_{i=1}^{n}(x_i - \overline{x})^2}\sqrt{\sum_{i=1}^{n}(y_i - \overline{y})^2}}. \tag{41}$$

It is useful for determining how well the ranking order of the values of one variable predict the ranking order of the values of the other variable.

The discrepancy between the AEL-AGL predictions and experiment is evaluated in terms of the normalized root-mean-square relative deviation

$$\mathrm{RMSrD} = \sqrt{\frac{\sum_{i=1}^{n}\left(\frac{X_i - Y_i}{X_i}\right)^2}{N-1}}. \tag{42}$$

In contrast to the correlations described above, lower values of the RMSrD indicate better agreement with experiment. This measure is particularly useful for comparing predictions of the same property using different methodologies that may have very similar correlations with, but different deviations from, the experimental results.

III. RESULTS

We used the AEL-AGL methodology to calculate the mechanical and thermal properties, including the bulk modulus, shear modulus, Poisson ratio, Debye temperature, Grüneisen parameter, and thermal conductivity for a set of 74 materials with structures including diamond, zinc-blende, rock-salt, wurzite, rhombohedral, and body-centred tetragonal. The results have been compared to experimental values (where available), and the correlations between the calculated and experimental values were deduced. In cases where multiple experimental values are present in the literature, we used the most recently reported value, unless otherwise specified.

In Sec. II A, three different approximations for the bulk and shear moduli are described: Voigt [Eqs. (2) and (3)], Reuss [Eqs. (4) and (5)], and the Voigt-Reuss-Hill (VRH) average [Eqs. (6) and (7)]. These approximations give very similar values for the bulk modulus for the set of materials included in this work, particularly those with cubic symmetry. Therefore only $B_{\mathrm{VRH}}^{\mathrm{AEL}}$ is explicitly cited in the following listed results (the values obtained for all three approximations are available in the AFLOW database entries for these materials). The values for the shear modulus in these three approximations exhibit larger variations, and are therefore all listed and compared to experiment. In several cases, the experimental values of the bulk and shear moduli have been calculated from the measured elastic constants using Eqs. (2) through (7), and an experimental Poisson ratio σ^{exp} was calculated from these values using Eq. (8).

As described in Sec. II C, the bulk modulus in AGL can be calculated from a polynomial fit of the $E(V)$ data as shown in Eq. (16), or by fitting the $E(V)$ data to one of three empirical equations of state: Birch-Murnaghan [Eq. (21)], Vinet [Eq. (23)], and the Baonza-Cáceres-Núñez [Eq. (26)]. We compare the results of these four methods, labeled $B_{\mathrm{Static}}^{\mathrm{AGL}}$, $B_{\mathrm{Static}}^{\mathrm{BM}}$, $B_{\mathrm{Static}}^{\mathrm{Vinet}}$, and $B_{\mathrm{Static}}^{\mathrm{BCN}}$, respectively, with the experimental values B^{exp} and those obtained from the elastic calculations $B_{\mathrm{VRH}}^{\mathrm{AEL}}$. The Debye temperatures, Grüneisen parameters and thermal conductivities depend on the calculated bulk modulus and are therefore also cited below for each of the equations of state. Also included are the Debye temperatures derived from the calculated elastic constants and speed of sound as given by Eq. (11). The Debye temperatures: $\theta_{\mathrm{D}}^{\mathrm{BM}}$ [Eq. (21)], $\theta_{\mathrm{D}}^{\mathrm{Vinet}}$ [Eq. (23)], and $\theta_{\mathrm{D}}^{\mathrm{BCN}}$, [Eq. (26)], calculated using the Poisson ratio σ^{AEL} obtained from Eq. (8), are compared to $\theta_{\mathrm{D}}^{\mathrm{AGL}}$, obtained from the numerical fit of $E(V)$ [Eq. (16)] using both σ^{AEL} and the approximation $\sigma = 0.25$ used in Ref. [34], to $\theta_{\mathrm{D}}^{\mathrm{AEL}}$, calculated with the speed of sound obtained using Eq. (11), and to the experimental values θ^{exp}. The values of the acoustic Debye temperature [θ_{a}, Eq. (38)] are shown, where available, in parentheses below the traditional Debye temperature value.

The experimental Grüneisen parameter, γ^{exp}, is compared to γ^{AGL} [Eq. (16)], obtained using the numerical polynomial fit of $E(V)$ and both values of the Poisson ratio (σ^{AEL} and the approximation $\sigma = 0.25$ from Ref. [34]), and to γ^{BM} [Eq. (21)], γ^{Vinet} [Eq. (23)], and γ^{BCN} [Eq. (26)], calculated using σ^{AEL} only. Similarly, the experimental lattice thermal conductivity κ^{exp} is compared to κ^{AGL} [Eq. (16)], obtained using the numerical polynomial fit and both the calculated and approximated values of σ, and to κ^{BM} [Eq. (21)], κ^{Vinet} [Eq. (23)], and κ^{BCN} [Eq. (26)], calculated using only σ^{AEL}.

The AEL method has been previously implemented in the Materials Project framework for calculating elastic constants [14]. Data from the Materials Project database are included in the tables below for comparison for the bulk modulus $B_{\mathrm{VRH}}^{\mathrm{MP}}$, shear modulus $G_{\mathrm{VRH}}^{\mathrm{MP}}$, and Poisson ratio σ^{MP}.

A. Zinc-blende and diamond structure materials

The mechanical and thermal properties were calculated for a set of materials with the zinc-blende (space group: $F\overline{4}3m$, No. 216; Pearson symbol: cF8; AFLOW prototype:

TABLE I. Bulk modulus, shear modulus, and Poisson ratio of zinc-blende (AFLOW prototype: AB_cF8_216_c_a [62]) and diamond (A_cF8_227_a [62]) structure semiconductors. "N/A"= Not available for that source. Units: B and G in GPa.

Comp.	B^{exp}	$B^{\text{AEL}}_{\text{VRH}}$	$B^{\text{MP}}_{\text{VRH}}$	$B^{\text{AGL}}_{\text{Static}}$	$B^{\text{BM}}_{\text{Static}}$	$B^{\text{Vinet}}_{\text{Static}}$	$B^{\text{BCN}}_{\text{Static}}$	G^{exp}	$G^{\text{AEL}}_{\text{Voigt}}$	$G^{\text{AEL}}_{\text{Reuss}}$	$G^{\text{AEL}}_{\text{VRH}}$	$G^{\text{MP}}_{\text{VRH}}$	σ^{exp}	σ^{AEL}	σ^{MP}
C	442 [66–68]	434	N/A	408	409	403	417	534 [66,68]	520	516	518	N/A	0.069 [66,68]	0.073	N/A
SiC	248 [69]	212	211	203	207	206	206	196 [70]	195	178	187	187	0.145 [67,70]	0.160	0.16
	211 [66,67]							170 [66]					0.183 [66]		
Si	97.8 [66,71]	89.1	83.0	84.2	85.9	85.0	86.1	66.5 [66,71]	64	61	62.5	61.2	0.223 [66,71]	0.216	0.2
	98 [67]														
Ge	75.8 [66,72]	61.5	59.0	54.9	55.7	54.5	56.1	55.3 [66,72]	47.7	44.8	46.2	45.4	0.207 [66,72]	0.199	0.19
	77.2 [67]														
BN	367.0 [67]	372	N/A	353	356	348	359	N/A	387	374	380	N/A	N/A	0.119	N/A
BP	165.0 [66,67]	162	161	155	157	156	157	136 [66,73]	164	160	162	162	0.186 [66,73]	0.125	0.12
	267 [66,74]														
	172 [66,73]														
AlP	86.0 [67]	82.9	85.2	78.9	80.4	79.5	80.4	N/A	48.6	44.2	46.4	47.2	N/A	0.264	0.27
AlAs	77.0 [67]	67.4	69.8	63.8	65.1	64.0	65.3	N/A	41.1	37.5	39.3	39.1	N/A	0.256	0.26
	74 [75]														
AlSb	58.2 [66,67,76,77]	49.4	49.2	46.5	47.8	46.9	47.8	31.9 [66,76,77]	29.7	27.4	28.5	29.6	0.268 [66,76,77]	0.258	0.25
GaP	88.7 [67]	78.8	76.2	71.9	73.4	72.2	73.8	55.3 [78]	53.5	49.1	51.3	51.8	0.244 [78]	0.232	0.22
	89.8 [78]														
GaAs	74.8 [67]	62.7	60.7	56.8	57.7	56.6	58.1	46.6 [79]	42.6	39.1	40.8	40.9	0.244 [79]	0.233	0.23
	75.5 [79]														
GaSb	57.0 [67]	47.0	44.7	41.6	42.3	41.2	42.6	34.2 [78]	30.8	28.3	29.6	30.0	0.248 [78]	0.240	0.23
	56.3 [78]														
InP	71.1 [67,80]	60.4	N/A	56.4	57.6	56.3	57.8	34.3 [80]	33.6	29.7	31.6	N/A	0.292 [80]	0.277	N/A
InAs	60.0 [67]	50.1	49.2	45.7	46.6	45.4	46.9	29.5 [66,81]	27.3	24.2	25.7	25.1	0.282 [66,81]	0.281	0.28
	57.9 [66,81]														
InSb	47.3 [67,82]	38.1	N/A	34.3	35.0	34.1	35.2	22.1 [82]	21.3	19.0	20.1	N/A	0.298 [82]	0.275	N/A
	48.3 [66,83]							23.7 [66,83]					0.289 [66,83]		
	46.5 [84]														
ZnS	77.1 [67]	71.2	68.3	65.8	66.1	65.2	66.6	30.9 [66]	36.5	31.4	33.9	33.2	0.318 [66]	0.294	0.29
	74.5 [66]														
ZnSe	62.4 [67,85]	58.2	58.3	53.3	53.8	52.8	54.1	29.1 [85]	29.5	25.6	27.5	27.5	0.298 [85]	0.296	0.3
ZnTe	51.0 [67,85]	43.8	46.0	39.9	40.5	39.4	40.7	23.4 [85]	23.3	20.8	22.1	22.4	0.30 [85]	0.284	0.29
CdSe	53.0 [67]	46.7	44.8	41.5	42.1	41.1	42.3	N/A	16.2	13.1	14.7	15.3	N/A	0.358	0.35
CdTe	42.4 [67]	36.4	35.3	32.2	32.7	31.9	32.8	N/A	14.2	11.9	13.0	13.6	N/A	0.340	0.33
HgSe	50.0 [67]	43.8	41.2	39.0	39.7	38.5	39.9	14.8 [86]	15.6	11.9	13.7	13.3	0.361 [86]	0.358	0.35
	48.5 [86]														
HgTe	42.3 [66,67,87]	35.3	N/A	31.0	31.6	30.8	31.9	14.7 [66,87]	14.4	11.6	13.0	N/A	0.344 [66,87]	0.335	N/A

AB_cF8_216_c_a [62,63]) and diamond ($Fd\bar{3}m$, No. 227; cF8; A_cF8_227_a [62,64]) structures. This is the same set of materials as in Table I of Ref. [34], which in turn are from Table II of Ref. [53] and Table 2.2 of Ref. [54].

The elastic properties bulk modulus, shear modulus and Poisson ratio calculated using AEL and AGL are shown in Table I and Fig. 1, together with experimental values from the literature where available. As can be seen from the results in Table I and Fig. 1(a), the $B^{\text{AEL}}_{\text{VRH}}$ values are generally closest to experiment as shown by the RMSrD value of 0.13, producing an underestimate of the order of 10%. The AGL values from both the numerical fit and the empirical equations of state are generally very similar to each other, while being slightly less than the $B^{\text{AEL}}_{\text{VRH}}$ values.

For the shear modulus, the experimental values G^{exp} are compared to the AEL values $G^{\text{AEL}}_{\text{Voigt}}$, $G^{\text{AEL}}_{\text{Reuss}}$, and $G^{\text{AEL}}_{\text{VRH}}$. As can be seen from the values in Table I and Fig. 1(b), the agreement with the experimental values is generally good with a very low RMSrD of 0.111 for $G^{\text{AEL}}_{\text{VRH}}$, with the Voigt approximation tending to overestimate and the Reuss approximation tending to underestimate, as would be expected. The experimental values of the Poisson ratio σ^{exp} and the AEL values σ^{AEL} [Eq. (8)] are also shown in Table I and Fig. 1(c), and the values are generally in good agreement. The Pearson [i.e., linear, Eq. (40)] and Spearman [i.e., rank order, Eq. (41)] correlations between all of the AEL-AGL elastic property values and experiment are shown in Table III, and are generally very high for all of these properties, ranging from 0.977 and 0.982, respectively, for σ^{exp} versus σ^{AEL}, up to 0.999 and 0.992 for B^{exp} versus $B^{\text{AEL}}_{\text{VRH}}$. These very high correlation values demonstrate the validity of using the AEL-AGL methodology to predict the elastic and mechanical properties of materials.

The Materials Project values of $B^{\text{MP}}_{\text{VRH}}$, $G^{\text{MP}}_{\text{VRH}}$, and σ^{MP} for diamond and zinc-blende structure materials are also shown in Table I, where available. The Pearson correlations values for the experimental results with the available values of $B^{\text{MP}}_{\text{VRH}}$, $G^{\text{MP}}_{\text{VRH}}$, and σ^{MP} were calculated to be 0.995, 0.987, and 0.952, respectively, while the respective Spearman correlations

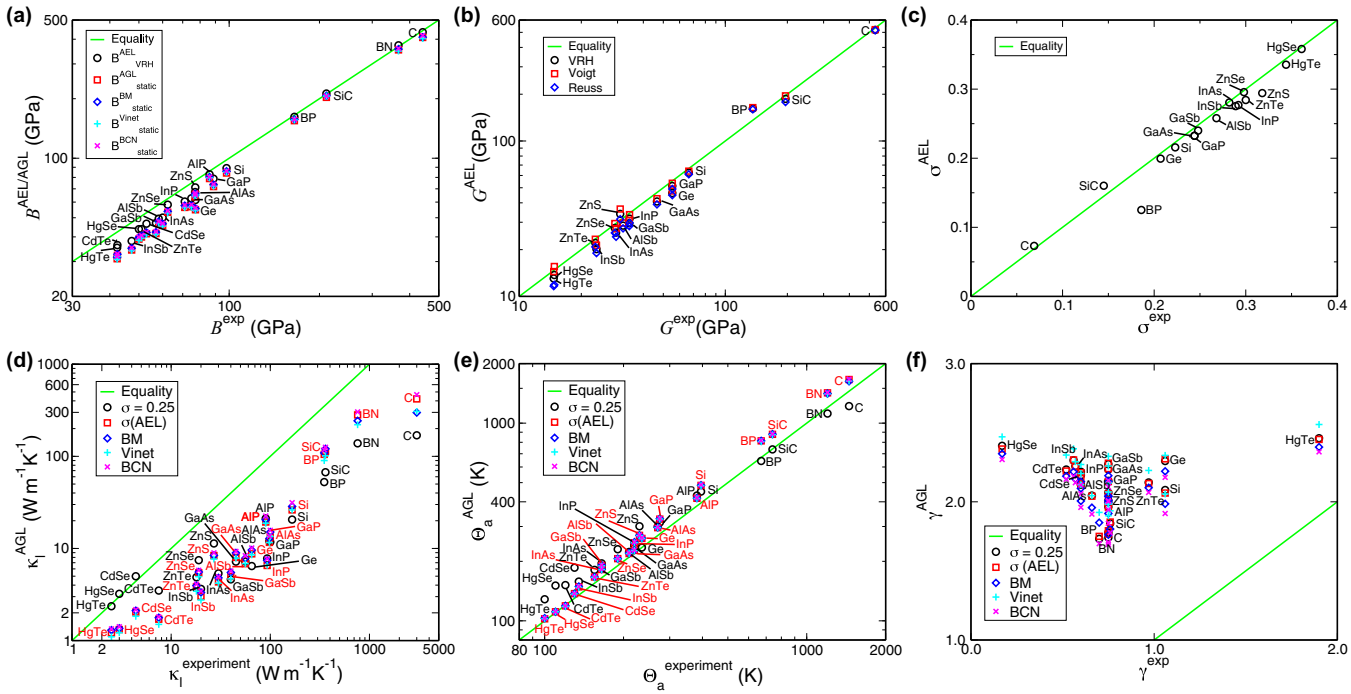

FIG. 1. (a) Bulk modulus, (b) shear modulus, (c) Poisson ratio, (d) lattice thermal conductivity at 300 K, (e) acoustic Debye temperature, and (f) Grüneisen parameter of zinc-blende (AFLOW prototype: AB_cF8_216_c_a [62]) and diamond (A_cF8_227_a [62]) structure semiconductors.

were 0.963, 0.977, and 0.977, and the RMSrD values were 0.149, 0.116 and 0.126. For comparison, the corresponding Pearson correlations for the same subset of materials for $B_{\rm VRH}^{\rm AEL}$, $G_{\rm VRH}^{\rm AEL}$, and $\sigma^{\rm AEL}$ are 0.997, 0.987, and 0.957, respectively, while the respective Spearman correlations were 0.982, 0.977, and 0.977, and the RMSrD values were 0.129, 0.114, and 0.108. These correlation values are very similar, and the general close agreement for $B_{\rm VRH}^{\rm AEL}$, $G_{\rm VRH}^{\rm AEL}$, and $\sigma^{\rm AEL}$ with $B_{\rm VRH}^{\rm MP}$, $G_{\rm VRH}^{\rm MP}$, and $\sigma^{\rm MP}$ demonstrate that the small differences in the parameters used for the DFT calculations make little difference to the results, indicating that the parameter set used here is robust for high-throughput calculations.

The thermal properties Debye temperature, Grüneisen parameter and thermal conductivity calculated using AGL for this set of materials are compared to the experimental values taken from the literature in Table II and are also plotted in Fig. 1. For the Debye temperature, the experimental values $\theta^{\rm exp}$ are compared to $\theta_{\rm D}^{\rm AGL}$, $\theta_{\rm D}^{\rm BM}$, $\theta_{\rm D}^{\rm Vinet}$, and $\theta_{\rm D}^{\rm BCN}$ in Fig. 1(e), while the values for the empirical equations of state are provided in Ref. [65]. Note that the $\theta^{\rm exp}$ values taken from Refs. [53,54] are for $\theta_{\rm a}$, and generally are in good agreement with the $\theta_{\rm a}^{\rm AGL}$ values. The values obtained using the numerical $E(V)$ fit and the three different equations of state are also in good agreement with each other, whereas the values of $\theta_{\rm D}^{\rm AGL}$ calculated using different σ values differ significantly, indicating that for this property the value of σ used is far more important than the equation of state used. The correlation between $\theta^{\rm exp}$ and the various AGL values is also very high, of the order of 0.999, and the RMSrD is low, of the order of 0.13.

The experimental values $\gamma^{\rm exp}$ of the Grüneisen parameter are plotted against $\gamma^{\rm AGL}$, $\gamma^{\rm BM}$, $\gamma^{\rm Vinet}$, and $\gamma^{\rm BCN}$ in Fig. 1(f), and the values are listed in Table II and in Ref. [65]. The very high RMSrD values (see Table III) show that AGL has problems accurately predicting the Grüneisen parameter for this set of materials, as the calculated value is often 2 to 3 times larger than the experimental one. Note also that there are quite large differences between the values obtained for different equations of state, with $\gamma^{\rm BCN}$ generally having the lowest values while $\gamma^{\rm Vinet}$ has the highest values. On the other hand, in contrast to the case of $\theta_{\rm D}^{\rm AGL}$, the value of σ used makes little difference to the value of $\gamma^{\rm AGL}$. The correlations between $\gamma^{\rm exp}$ and the AGL values, as shown in Table III, are also quite poor, with no value higher than 0.2 for the Pearson correlations, and negative Spearman correlations.

The experimental thermal conductivity $\kappa^{\rm exp}$ is compared in Fig. 1(d) to the thermal conductivities calculated with AGL using the Leibfried-Schlömann equation (37): $\kappa^{\rm AGL}$, $\kappa^{\rm BM}$, $\kappa^{\rm Vinet}$, and $\kappa^{\rm BCN}$, while the values are listed in Table II and in Ref. [65]. The absolute agreement between the AGL values and $\kappa^{\rm exp}$ is quite poor, with RMSrD values of the order of 0.8 and discrepancies of tens, or even hundreds, of percent quite common. Considerable disagreements also exist between different experimental reports of these properties, in almost all cases where they exist. Unfortunately, the scarcity of experimental data from different sources on the thermal properties of these materials prevents reaching definite conclusions regarding the true values of these properties. The available data can thus only be considered as a rough indication of their order of magnitude.

The Pearson correlations between the AGL calculated thermal conductivity values and the experimental values are high, ranging from 0.871 to 0.932, while the Spearman correlations are even higher, ranging from 0.905 to 0.954, as shown in Table III. In particular, note that using the $\sigma^{\rm AEL}$ in

TABLE II. Thermal properties lattice thermal conductivity at 300 K, Debye temperature, and Grüneisen parameter of zinc-blende (AFLOW prototype: AB_cF8_216_c_a [62]) and diamond (A_cF8_227_a [62]) structure semiconductors, comparing the effect of using the calculated value of the Poisson ratio to the previous approximation of $\sigma = 0.25$. The values listed for θ^{exp} are θ_{a}, except 141 K for HgTe, which is θ_{D} [88]. Units: κ in W m^{-1} K^{-1} and θ in Kelvin.

Comp.	κ^{exp}	κ^{AGL} ($\sigma = 0.25$) [34]	κ^{AGL}	θ^{exp}	$\theta_{\text{D}}^{\text{AGL}}$ ($\theta_{\text{a}}^{\text{AGL}}$) ($\sigma = 0.25$) [34]	$\theta_{\text{D}}^{\text{AGL}}$ ($\theta_{\text{a}}^{\text{AGL}}$)	$\theta_{\text{D}}^{\text{AEL}}$	γ^{exp}	γ^{AGL} ($\sigma = 0.25$) [34]	γ^{AGL}
C	3000 [54]	169.1	419.9	1450 [53,54]	1536 (1219)	2094 (1662)	2222	0.75 [54] 0.9 [53]	1.74	1.77
SiC	360 [89]	67.19	113.0	740 [53]	928 (737)	1106 (878)	1143	0.76 [53]	1.84	1.85
Si	166 [54]	20.58	26.19	395 [53,54]	568 (451)	610 (484)	624	1.06 [54] 0.56 [53]	2.09	2.06
Ge	65 [54]	6.44	8.74	235 [53,54]	296 (235)	329 (261)	342	1.06 [54] 0.76 [53]	2.3	2.31
BN	760 [54]	138.4	281.6	1200 [54]	1409 (1118)	1793 (1423)	1887	0.7 [54]	1.73	1.75
BP	350 [54]	52.56	105.0	670 [53,54]	811 (644)	1025 (814)	1062	0.75 [54]	1.78	1.79
AlP	90 [90,91]	21.16	19.34	381 [54]	542 (430)	525 (417)	531	0.75 [54]	1.96	1.96
AlAs	98 [54]	12.03	11.64	270 [53,54]	378 (300)	373 (296)	377	0.66 [53,54]	2.04	2.04
AlSb	56 [54]	7.22	6.83	210 [53,54]	281 (223)	276 (219)	277	0.6 [53,54]	2.12	2.13
GaP	100 [54]	11.76	13.34	275 [53,54]	396 (314)	412 (327)	423	0.75 [54] 0.76 [53]	2.15	2.15
GaAs	45 [54]	7.2	8.0	220 [53,54]	302 (240)	313 (248)	322	0.75 [53,54]	2.23	2.24
GaSb	40 [54]	4.62	4.96	165 [53,54]	234 (186)	240 (190)	248	0.75 [53,54]	2.27	2.28
InP	93 [54]	7.78	6.53	220 [53,54]	304 (241)	286 (227)	287	0.6 [53,54]	2.22	2.21
InAs	30 [54]	5.36	4.33	165 [53,54]	246 (195)	229 (182)	231	0.57 [53,54]	2.26	2.26
InSb	20 [54] 16.5 [88]	3.64	3.02	135 [53,54]	199 (158)	187 (148)	190	0.56 [53,54]	2.3	2.3
ZnS	27 [54]	11.33	8.38	230 [53,54]	379 (301)	341 (271)	346	0.75 [53,54]	2.01	2.00
ZnSe	19 [54] 33 [88]	7.46	5.44	190 [53,54]	290 (230)	260 (206)	263	0.75 [53,54]	2.07	2.06
ZnTe	18 [54]	4.87	3.83	155 [53,54]	228 (181)	210 (167)	212	0.97 [53,54]	2.14	2.13
CdSe	4.4 [88]	4.99	2.04	130 [54]	234 (186)	173 (137)	174	0.6 [54]	2.19	2.18
CdTe	7.5 [54]	3.49	1.71	120 [53,54]	191 (152)	150 (119)	152	0.52 [53,54]	2.23	2.22
HgSe	3 [92]	3.22	1.32	110 [53]	190 (151)	140 (111)	140	0.17 [53]	2.4	2.38
HgTe	2.5 [88]	2.36	1.21	141 [88] (100) [53]	162 (129)	129 (102)	130	1.9 [88]	2.46	2.45

the AGL calculations improves the correlations by about 5%, from 0.878 to 0.927 and from 0.905 to 0.95. For the different equations of state, κ^{AGL} and κ^{BCN} appear to correlate better with κ^{exp} than κ^{BM} and κ^{Vinet} for this set of materials.

As we noted in our previous work on AGL [34], some of the inaccuracy in the thermal conductivity results may be due to the inability of the Leibfried-Schlömann equation to fully describe effects such as the suppression of phonon-phonon scattering due to large gaps between the branches of the phonon dispersion [26]. This can be seen from the thermal conductivity values shown in Table 2.2 of Ref. [54] calculated using the experimental values of θ_{a} and γ in the Leibfried-Schlömann equation. There are large discrepancies in certain cases such as diamond, while the Pearson and Spearman correlations of

TABLE III. Correlations and deviations between experimental values and AEL and AGL results for elastic and thermal properties for zinc-blende and diamond structure semiconductors.

Property	Pearson (Linear)	Spearman (Rank Order)	RMSrD
$\kappa^{\rm exp}$ versus $\kappa^{\rm AGL}$ ($\sigma = 0.25$) [34]	0.878	0.905	0.776
$\kappa^{\rm exp}$ versus $\kappa^{\rm AGL}$	0.927	0.95	0.796
$\kappa^{\rm exp}$ versus $\kappa^{\rm BM}$	0.871	0.954	0.787
$\kappa^{\rm exp}$ versus $\kappa^{\rm Vinet}$	0.908	0.954	0.815
$\kappa^{\rm exp}$ versus $\kappa^{\rm BCN}$	0.932	0.954	0.771
$\theta_{\rm a}^{\rm exp}$ versus $\theta_{\rm a}^{\rm AGL}$ ($\sigma = 0.25$) [34]	0.995	0.984	0.200
$\theta_{\rm a}^{\rm exp}$ versus $\theta_{\rm a}^{\rm AGL}$	0.999	0.998	0.132
$\theta_{\rm a}^{\rm exp}$ versus $\theta_{\rm a}^{\rm BM}$	0.999	0.998	0.132
$\theta_{\rm a}^{\rm exp}$ versus $\theta_{\rm a}^{\rm Vinet}$	0.999	0.998	0.127
$\theta_{\rm a}^{\rm exp}$ versus $\theta_{\rm a}^{\rm BCN}$	0.999	0.998	0.136
$\gamma^{\rm exp}$ versus $\gamma^{\rm AGL}$ ($\sigma = 0.25$) [34]	0.137	−0.187	3.51
$\gamma^{\rm exp}$ versus $\gamma^{\rm AGL}$	0.145	−0.165	3.49
$\gamma^{\rm exp}$ versus $\gamma^{\rm BM}$	0.169	−0.178	3.41
$\gamma^{\rm exp}$ versus $\gamma^{\rm Vinet}$	0.171	−0.234	3.63
$\gamma^{\rm exp}$ versus $\gamma^{\rm BCN}$	0.144	−0.207	3.32
$B^{\rm exp}$ versus $B_{\rm VRH}^{\rm AEL}$	0.999	0.992	0.130
$B^{\rm exp}$ versus $B_{\rm Static}^{\rm AGL}$	0.999	0.986	0.201
$B^{\rm exp}$ versus $B_{\rm Static}^{\rm BM}$	0.999	0.986	0.189
$B^{\rm exp}$ versus $B_{\rm Static}^{\rm Vinet}$	0.999	0.986	0.205
$B^{\rm exp}$ versus $B_{\rm Static}^{\rm BCN}$	0.999	0.986	0.185
$G^{\rm exp}$ versus $G_{\rm VRH}^{\rm AEL}$	0.998	0.980	0.111
$G^{\rm exp}$ versus $G_{\rm Voigt}^{\rm AEL}$	0.998	0.980	0.093
$G^{\rm exp}$ versus $G_{\rm Reuss}^{\rm AEL}$	0.998	0.980	0.152
$\sigma^{\rm exp}$ versus $\sigma^{\rm AEL}$	0.977	0.982	0.095

0.932 and 0.941 respectively are very similar to the correlations we calculated using the AGL evaluations of $\theta_{\rm a}$ and γ.

Thus the unsatisfactory quantitative reproduction of these quantities by the Debye quasiharmonic model has little impact on its effectiveness as a screening tool for identifying high or low thermal conductivity materials. The model can be used when these experimental values are unavailable to help determine the relative values of these quantities and for ranking materials conductivity.

B. Rock-salt structure materials

The mechanical and thermal properties were calculated for a set of materials with the rock-salt structure (space group: $Fm\overline{3}m$, No. 225; Pearson symbol: cF8; AFLOW prototype: AB_cF8_225_a_b [62,93]). This is the same set of materials as in Table II of Ref. [34], which in turn are from the sets in Table III of Ref. [53] and Table 2.1 of Ref. [54].

The elastic properties of bulk modulus, shear modulus and Poisson ratio, as calculated using AEL and AGL are shown in Table IV and Fig. 2, together with experimental values from the literature where available. As can be seen from the results in Table IV and Fig. 2(a), for this set of materials the $B_{\rm VRH}^{\rm AEL}$ values are closest to experiment, with an RMSrD of 0.078. The AGL values from both the numerical fit and the empirical equations of state are generally very similar to each other, while being slightly less than the $B_{\rm VRH}^{\rm AEL}$ values.

For the shear modulus, the experimental values $G^{\rm exp}$ are compared to the AEL values $G_{\rm Voigt}^{\rm AEL}$, $G_{\rm Reuss}^{\rm AEL}$, and $G_{\rm VRH}^{\rm AEL}$. As can be seen from the values in Table IV and Fig. 2(b), the agreement with the experimental values is generally good with an RMSrD of 0.105 for $G_{\rm VRH}^{\rm AEL}$, with the Voigt approximation tending to overestimate and the Reuss approximation tending to underestimate, as would be expected. The experimental values of the Poisson ratio $\sigma^{\rm exp}$ and the AEL values $\sigma^{\rm AEL}$ [see Eq. (8)] are also shown in Table IV and Fig. 2(c), and the values are generally in good agreement. The Pearson [i.e., linear, Eq. (40)] and Spearman [i.e., rank order, Eq. (41)] correlations between all of the AEL-AGL elastic property values and experiment are shown in Table VI, and are generally very high for all of these properties, ranging from 0.959 and 0.827, respectively, for $\sigma^{\rm exp}$ versus $\sigma^{\rm AEL}$, up to 0.998 and 0.995 for $B^{\rm exp}$ versus $B_{\rm VRH}^{\rm AEL}$. These very high correlation values demonstrate the validity of using the AEL-AGL methodology to predict the elastic and mechanical properties of materials.

The values of $B_{\rm VRH}^{\rm MP}$, $G_{\rm VRH}^{\rm MP}$, and $\sigma^{\rm MP}$ for rock-salt structure materials are also shown in Table IV, where available. The Pearson correlations for the experimental results with the available values of $B_{\rm VRH}^{\rm MP}$, $G_{\rm VRH}^{\rm MP}$, and $\sigma^{\rm MP}$ were calculated to be 0.997, 0.994, and 0.890, respectively, while the respective Spearman correlations were 0.979, 0.998, and 0.817, and the RMSrD values were 0.153, 0.105, and 0.126. For comparison, the corresponding Pearson correlations for the same subset of materials for $B_{\rm VRH}^{\rm AEL}$, $G_{\rm VRH}^{\rm AEL}$, and $\sigma^{\rm AEL}$ are 0.998, 0.995, and 0.951, respectively, while the respective Spearman correlations were 0.996, 1.0, and 0.843, and the RMSrD values were 0.079, 0.111, and 0.071. These correlation values are very similar, and the general close agreement for the results for the values of $B_{\rm VRH}^{\rm AEL}$, $G_{\rm VRH}^{\rm AEL}$, and $\sigma^{\rm AEL}$ with those of $B_{\rm VRH}^{\rm MP}$, $G_{\rm VRH}^{\rm MP}$, and $\sigma^{\rm MP}$ demonstrate that the small differences in the parameters used for the DFT calculations make little difference to the results, indicating that the parameter set used here is robust for high-throughput calculations.

The thermal properties of Debye temperature, Grüneisen parameter and thermal conductivity calculated using AGL are compared to the experimental values taken from the literature in Table V and are also plotted in Fig. 2. For the Debye temperature, the experimental values $\theta^{\rm exp}$ are compared to $\theta_{\rm D}^{\rm AGL}$, $\theta_{\rm D}^{\rm BM}$, $\theta_{\rm D}^{\rm Vinet}$, and $\theta_{\rm D}^{\rm BCN}$ in Fig. 2(e), while the actual values for the empirical equations of state are provided in Ref. [65]. Note that the $\theta^{\rm exp}$ values taken from Ref. [53,54] are for $\theta_{\rm a}$, and generally are in good agreement with the $\theta_{\rm a}^{\rm AGL}$ values. The values obtained using the numerical $E(V)$ fit and the three different equations of state are also in good agreement with each other, whereas the values of $\theta_{\rm D}^{\rm AGL}$ calculated using different σ values differ significantly, indicating that, as in the case of the zinc-blende and diamond structures, the value of σ used is far more important for this property than the equation of state used. The correlation between $\theta^{\rm exp}$ and the various AGL values is also quite high, of the order of 0.98 for the Pearson correlation and 0.92 for the Spearman correlation.

The experimental values $\gamma^{\rm exp}$ of the Grüneisen parameter are plotted against $\gamma^{\rm AGL}$, $\gamma^{\rm BM}$, $\gamma^{\rm Vinet}$, and $\gamma^{\rm BCN}$ in Fig. 2(f), and the values are listed in Table V and in Ref. [65]. These results show that AGL has problems accurately predicting

TABLE IV. Mechanical properties bulk modulus, shear modulus and Poisson ratio of rock-salt (AFLOW Prototype: AB_cF8_225_a_b [62]) structure semiconductors. "N/A" = Not available for that that source. Units: B and G in GPa.

Comp.	$B^{\rm exp}$	$B^{\rm AEL}_{\rm VRH}$	$B^{\rm MP}_{\rm VRH}$	$B^{\rm AGL}_{\rm Static}$	$B^{\rm BM}_{\rm Static}$	$B^{\rm Vinet}_{\rm Static}$	$B^{\rm BCN}_{\rm Static}$	$G^{\rm exp}$	$G^{\rm AEL}_{\rm Voigt}$	$G^{\rm AEL}_{\rm Reuss}$	$G^{\rm AEL}_{\rm VRH}$	$G^{\rm MP}_{\rm VRH}$	$\sigma^{\rm exp}$	$\sigma^{\rm AEL}$	$\sigma^{\rm MP}$
LiH	33.7 [94]	37.7	36.1	29.5	29.0	27.7	31.4	36.0 [94]	43.4	42.3	42.8	42.9	0.106 [94]	0.088	0.07
LiF	69.6 [95]	70.4	69.9	58.6	59.9	57.5	61.2	48.8 [95]	46.4	45.8	46.1	50.9	0.216 [95]	0.231	0.21
NaF	48.5 [95]	46.9	47.6	38.7	38.6	36.8	39.3	31.2 [95]	29.5	28.4	28.9	30.0	0.236 [95]	0.244	0.24
NaCl	25.1 [95]	24.9	22.6	20.0	20.5	19.2	20.7	14.6 [95]	14.0	12.9	13.5	14.3	0.255 [95]	0.271	0.24
NaBr	20.6 [95]	20.5	27.1	16.3	16.9	15.7	16.9	11.6 [95]	11.0	9.9	10.4	11.6	0.264 [95]	0.283	0.31
NaI	15.95 [95]	16.4	15.8	12.6	13.2	12.2	13.1	8.59 [95]	8.35	7.31	7.83	8.47	0.272 [95]	0.295	0.27
KF	31.6 [95]	29.9	28.9	25.1	24.2	22.9	24.7	16.7 [95]	16.5	15.4	15.9	16.5	0.275 [95]	0.274	0.26
KCl	18.2 [95]	16.7	15.8	13.8	13.7	12.7	13.6	9.51 [95]	10.1	8.51	9.30	9.24	0.277 [95]	0.265	0.26
KBr	15.4 [95]	13.8	21.6	11.1	11.4	10.5	11.2	7.85 [95]	8.14	6.46	7.30	7.33	0.282 [95]	0.276	0.35
KI	12.2 [95]	10.9	9.52	8.54	9.03	8.28	8.84	5.96 [95]	6.05	4.39	5.22	5.55	0.290 [95]	0.294	0.26
RbCl	16.2 [95]	14.3	14.6	12.1	11.8	11.0	11.8	7.63 [95]	8.06	6.41	7.24	7.67	0.297 [95]	0.284	0.28
RbBr	13.8 [95]	12.6	13.8	10.3	9.72	9.06	9.67	6.46 [95]	7.12	5.24	6.18	6.46	0.298 [95]	0.289	0.3
RbI	11.1 [95]	9.90	9.66	8.01	7.74	7.12	7.54	5.03 [95]	5.50	3.65	4.57	4.63	0.303 [95]	0.300	0.29
AgCl	44.0 [96]	40.6	N/A	33.7	34.1	33.0	34.7	8.03 [96]	8.68	8.66	8.67	N/A	0.414 [96]	0.400	N/A
MgO	164 [97]	152	152	142	142	140	144	131 [97]	119	115	117	119	0.185 [97]	0.194	0.19
CaO	113 [98]	105	105	99.6	100	98.7	101	81.0 [98]	73.7	73.7	73.7	74.2	0.210 [98]	0.216	0.21
SrO	91.2 [98]	84.7	87.4	80.0	80.2	79.1	80.8	58.7 [98]	55.1	55.0	55.1	56.0	0.235 [98]	0.233	0.24
BaO	75.4 [98]	69.1	68.4	64.6	64.3	63.0	64.6	35.4 [98]	36.4	36.4	36.4	37.8	0.297 [98]	0.276	0.27
PbS	52.9 [66,99]	53.5	N/A	49.9	50.8	50.0	51.0	27.9 [66,99]	34.0	26.8	30.4	N/A	0.276 [66,99]	0.261	N/A
PbSe	54.1 [66,100]	47.7	N/A	43.9	44.8	43.9	44.9	26.2 [66,100]	31.7	23.6	27.6	N/A	0.291 [66,100]	0.257	N/A
PbTe	39.8 [66,101]	39.5	N/A	36.4	36.6	35.8	36.8	23.1 [66,101]	28.7	19.8	24.3	N/A	0.256 [66,101]	0.245	N/A
SnTe	37.8 [66,102]	40.4	39.6	38.1	38.4	37.6	38.6	20.8 [66,102]	31.4	22.0	26.7	27.6	0.267 [66,102]	0.229	0.22

the Grüneisen parameter for this set of materials as well, as the calculated values are often 30% to 50% larger than the experimental ones and the RMSrD values are of the order of 0.5. Note also that there are quite large differences between the values obtained for different equations of state, with $\gamma^{\rm BCN}$ generally having the lowest values while $\gamma^{\rm Vinet}$ has the highest values, a similar pattern to that seen above for the zinc-blende and diamond structure materials. On the other

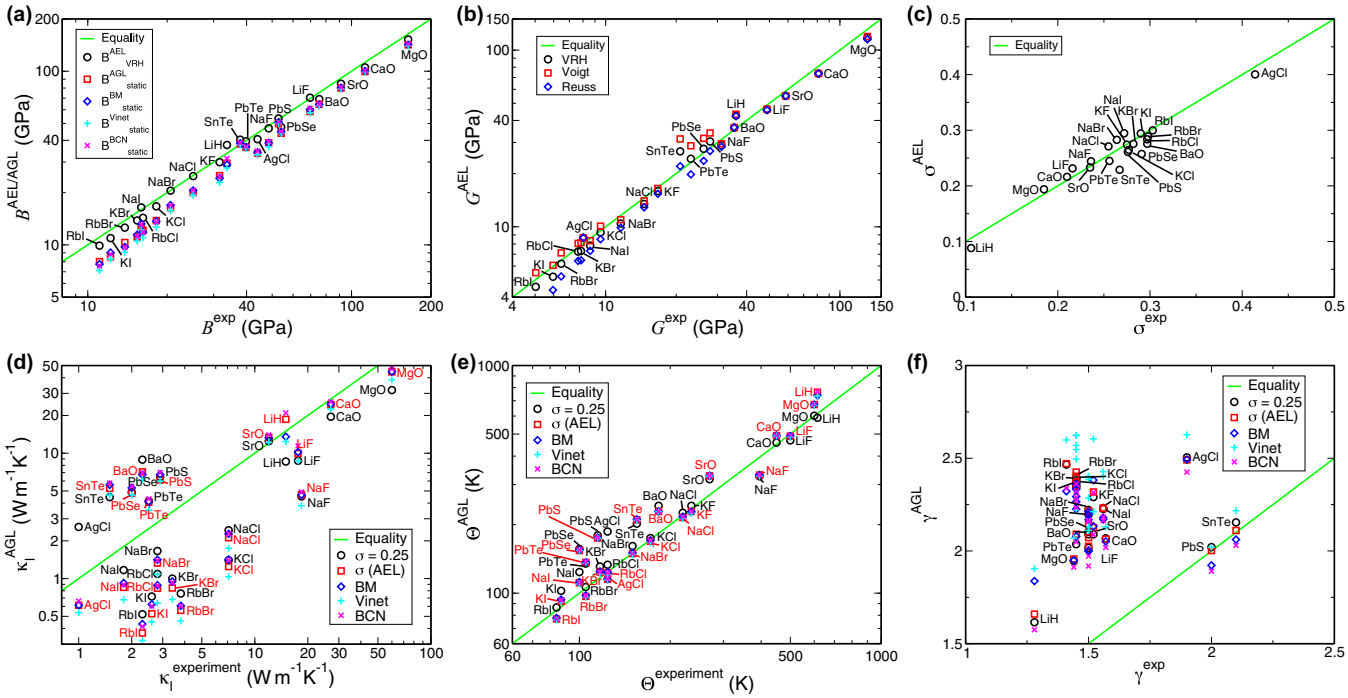

FIG. 2. (a) Bulk modulus, (b) shear modulus, (c) Poisson ratio, (d) lattice thermal conductivity at 300 K, (e) Debye temperature, and (f) Grüneisen parameter of rock-salt structure (AFLOW Prototype: AB_cF8_225_a_b [62]) semiconductors. The Debye temperatures plotted in (b) are $\theta_{\rm a}$, except for SnTe where $\theta_{\rm D}$ is quoted in Ref. [88].

TABLE V. Thermal properties lattice thermal conductivity at 300 K, Debye temperature and Grüneisen parameter of rock-salt structure (AFLOW prototype: AB_cF8_225_a_b [62]) semiconductors, comparing the effect of using the calculated value of the Poisson ratio to previous approximation of $\sigma = 0.25$. The values listed for θ^{exp} are θ_{a}, except 155 K for SnTe, which is θ_{D} [88]. "N/A" = Not available for that source. Units: κ in W m^{-1} K^{-1} and θ in Kelvin.

Comp.	κ^{exp}	κ^{AGL} ($\sigma = 0.25$) [34]	κ^{AGL}	θ^{exp}	$\theta_{\mathrm{D}}^{\mathrm{AGL}}$ ($\theta_{\mathrm{a}}^{\mathrm{AGL}}$) ($\sigma = 0.25$) [34]	$\theta_{\mathrm{D}}^{\mathrm{AGL}}$ ($\theta_{\mathrm{a}}^{\mathrm{AGL}}$)	$\theta_{\mathrm{D}}^{\mathrm{AEL}}$	γ^{exp}	γ^{AGL} ($\sigma = 0.25$) [34]	γ^{AGL}
LiH	15 [54]	8.58	18.6	615 [53,54]	743 (590)	962 (764)	1175	1.28 [53,54]	1.62	1.66
LiF	17.6 [54]	8.71	9.96	500 [53,54]	591 (469)	617 (490)	681	1.5 [53,54]	2.02	2.03
NaF	18.4 [54]	4.52	4.67	395 [53,54]	411 (326)	416 (330)	455	1.5 [53,54]	2.2	2.21
NaCl	7.1 [54]	2.43	2.12	220 [53,54]	284 (225)	271 (215)	289	1.56 [53,54]	2.23	2.23
NaBr	2.8 [54]	1.66	1.33	150 [53,54]	203 (161)	188 (149)	198	1.5 [53,54]	2.22	2.22
NaI	1.8 [54]	1.17	0.851	100 [53,54]	156 (124)	140 (111)	147	1.56 [53,54]	2.23	2.23
KF	N/A	2.68	2.21	235 [53,54]	305 (242)	288 (229)	309	1.52 [53,54]	2.29	2.32
KCl	7.1 [54]	1.4	1.25	172 [53,54]	220 (175)	213 (169)	226	1.45 [53,54]	2.38	2.40
KBr	3.4 [54]	1.0	0.842	117 [53,54]	165 (131)	156 (124)	162	1.45 [53,54]	2.37	2.37
KI	2.6 [54]	0.72	0.525	87 [53,54]	129 (102)	116 (92)	120	1.45 [53,54]	2.35	2.35
RbCl	2.8 [54]	1.09	0.837	124 [53,54]	168 (133)	155 (123)	160	1.45 [53,54]	2.34	2.37
RbBr	3.8 [54]	0.76	0.558	105 [53,54]	134 (106)	122 (97)	129	1.45 [53,54]	2.40	2.43
RbI	2.3 [54]	0.52	0.368	84 [53,54]	109 (87)	97 (77)	102	1.41 [53,54]	2.47	2.47
AgCl	1.0 [90,103]	2.58	0.613	124 [53]	235 (187)	145 (115)	148	1.9 [53]	2.5	2.49
MgO	60 [54]	31.9	44.5	600 [53,54]	758 (602)	849 (674)	890	1.44 [53,54]	1.95	1.96
CaO	27 [54]	19.5	24.3	450 [53,54]	578 (459)	620 (492)	638	1.57 [53,54]	2.07	2.06
SrO	12 [54]	12.5	13.4	270 [53,54]	399 (317)	413 (328)	421	1.52 [53,54]	2.09	2.13
BaO	2.3 [54]	8.88	7.10	183 [53,54]	305 (242)	288 (229)	292	1.5 [53,54]	2.09	2.14
PbS	2.9 [54]	6.48	6.11	115 [53,54]	226 (179)	220 (175)	221	2.0 [53,54]	2.02	2.00
PbSe	2.0 [54]	4.88	4.81	100 [54]	197 (156)	194 (154)	196	1.5 [54]	2.1	2.07
PbTe	2.5 [54]	4.15	4.07	105 [53,54]	170 (135)	172 (137)	175	1.45 [53,54]	2.04	2.09
SnTe	1.5 [88]	4.46	5.24	155 [88]	202 (160)	210 (167)	212	2.1 [88]	2.15	2.11

hand, in contrast to the case of $\theta_{\mathrm{D}}^{\mathrm{AGL}}$, the value of σ used makes little difference to the value of γ^{AGL}. The correlation values between γ^{exp} and the AGL values, as shown in Table VI, are also quite poor, with values ranging from –0.098 to 0.118 for the Pearson correlations, and negative values for the Spearman correlations.

The experimental thermal conductivity κ^{exp} is compared in Fig. 2(d) to the thermal conductivities calculated with AGL using the Leibfried-Schlömann equation (37): κ^{AGL}, κ^{BM}, κ^{Vinet}, and κ^{BCN}, while the values are listed in Table V and in Ref. [65]. The linear correlation between the AGL values and κ^{exp} is somewhat better than for the zinc-blende materials set, with a Pearson correlation as high as 0.94, although the Spearman correlations are somewhat lower, ranging from 0.445 to 0.556. In particular, note that using the σ^{AEL} in the AGL calculations improves the correlations by

TABLE VI. Correlations between experimental values and AEL and AGL results for elastic and thermal properties for rock-salt structure semiconductors.

Property	Pearson (Linear)	Spearman (Rank Order)	RMSrD
$\kappa^{\rm exp}$ versus $\kappa^{\rm AGL}$ ($\sigma = 0.25$) [34]	0.910	0.445	1.093
$\kappa^{\rm exp}$ versus $\kappa^{\rm AGL}$	0.932	0.528	1.002
$\kappa^{\rm exp}$ versus $\kappa^{\rm BM}$	0.940	0.556	1.038
$\kappa^{\rm exp}$ versus $\kappa^{\rm Vinet}$	0.933	0.540	0.920
$\kappa^{\rm exp}$ versus $\kappa^{\rm BCN}$	0.930	0.554	1.082
$\theta^{\rm exp}$ versus $\theta^{\rm AGL}$ ($\sigma = 0.25$) [34]	0.985	0.948	0.253
$\theta^{\rm exp}$ versus $\theta^{\rm AGL}$	0.978	0.928	0.222
$\theta^{\rm exp}$ versus $\theta^{\rm BM}$	0.980	0.926	0.222
$\theta^{\rm exp}$ versus $\theta^{\rm Vinet}$	0.979	0.925	0.218
$\theta^{\rm exp}$ versus $\theta^{\rm BCN}$	0.978	0.929	0.225
$\gamma^{\rm exp}$ versus $\gamma^{\rm AGL}$ ($\sigma = 0.25$) [34]	0.118	−0.064	0.477
$\gamma^{\rm exp}$ versus $\gamma^{\rm AGL}$	0.036	−0.110	0.486
$\gamma^{\rm exp}$ versus $\gamma^{\rm BM}$	−0.019	−0.088	0.462
$\gamma^{\rm exp}$ versus $\gamma^{\rm Vinet}$	−0.098	−0.086	0.591
$\gamma^{\rm exp}$ versus $\gamma^{\rm BCN}$	0.023	−0.110	0.443
$B^{\rm exp}$ versus $B^{\rm AEL}_{\rm VRH}$	0.998	0.995	0.078
$B^{\rm exp}$ versus $B^{\rm AGL}_{\rm Static}$	0.998	0.993	0.201
$B^{\rm exp}$ versus $B^{\rm BM}_{\rm Static}$	0.997	0.993	0.199
$B^{\rm exp}$ versus $B^{\rm Vinet}_{\rm Static}$	0.997	0.990	0.239
$B^{\rm exp}$ versus $B^{\rm BCN}_{\rm Static}$	0.998	0.993	0.197
$G^{\rm exp}$ versus $G^{\rm AEL}_{\rm VRH}$	0.994	0.997	0.105
$G^{\rm exp}$ versus $G^{\rm AEL}_{\rm Voigt}$	0.991	0.990	0.157
$G^{\rm exp}$ versus $G^{\rm AEL}_{\rm Reuss}$	0.995	0.995	0.142
$\sigma^{\rm exp}$ versus $\sigma^{\rm AEL}$	0.959	0.827	0.070

about 2% to 8%, from 0.910 to 0.932 and from 0.445 to 0.528. For the different equations of state, the results for $\kappa^{\rm BM}$ appear to correlate best with $\kappa^{\rm exp}$ for this set of materials.

As in the case of the diamond and zinc-blende structure materials discussed in the previous section, Ref. [54] includes values of the thermal conductivity at 300 K for rock-salt structure materials, calculated using the experimental values of $\theta_{\rm a}$ and γ in the Leibfried-Schlömann equation, in Table 2.1. The correlation values of 0.986 and 0.761 with experiment are better than those obtained for the AGL results by a larger margin than for the zinc-blende materials. Nevertheless, the Pearson correlation between the calculated and experimental conductivities is high in both calculations, indicating that the AGL approach may be used as a screening tool for high- or low-conductivity compounds in cases where gaps exist in the experimental data for these materials.

C. Hexagonal structure materials

The experimental data for this set of materials appears in Table III of Ref. [34], taken from Table 2.3 of Ref. [54]. Most of these materials have the wurtzite structure ($P6_3mc$, No. 186; Pearson symbol: hP4; AFLOW prototype: AB_hP4_186_b_b [62,104]) except InSe which is $P6_3mmc$, No. 194, Pearson symbol: hP8.

The calculated elastic properties are shown in Table VII and Fig. 3. The bulk moduli values obtained from a direct calculation of the elastic tensor, $B^{\rm AEL}_{\rm VRH}$, are usually slightly higher than those obtained from the $E(V)$ curve and are also closer to experiment [Table VII and Fig. 3(a)], with the exception of InSe where it is noticeably lower.

For the shear modulus, the experimental values $G^{\rm exp}$ are compared to the AEL values $G^{\rm AEL}_{\rm Voigt}$, $G^{\rm AEL}_{\rm Reuss}$, and $G^{\rm AEL}_{\rm VRH}$. As can be seen in Table VII and Fig. 3(b), the agreement with the experimental values is very good. Similarly good agreement is obtained for the Poisson ratio of most materials [Table VII and Fig. 3(c)], with a single exception for InSe where the calculation deviates significantly from the experiment. The Pearson [i.e., linear, Eq. (40)] and Spearman [i.e., rank order, Eq. (41)] correlations between the calculated elastic properties and their experimental values are generally quite high (Table IX), ranging from 0.851 and 0.893, respectively, for $\sigma^{\rm exp}$ versus $\sigma^{\rm AEL}$, up to 0.998 and 1.0 for $G^{\rm exp}$ versus $G^{\rm AEL}_{\rm VRH}$.

The Materials Project values of $B^{\rm MP}_{\rm VRH}$, $G^{\rm MP}_{\rm VRH}$, and $\sigma^{\rm MP}$ for hexagonal structure materials are also shown in Table VII, where available. The Pearson correlations values for the experimental results with the available values of $B^{\rm MP}_{\rm VRH}$, $G^{\rm MP}_{\rm VRH}$, and $\sigma^{\rm MP}$ were calculated to be 0.984, 0.998, and 0.993, respectively, while the respective Spearman correlations were 0.943, 1.0, and 0.943, and the RMSrD values were 0.117, 0.116, and 0.034. For comparison, the corresponding Pearson correlations for the same subset of materials for $B^{\rm AEL}_{\rm VRH}$, $G^{\rm AEL}_{\rm VRH}$, and $\sigma^{\rm AEL}$ are 0.986, 0.998, and 0.998 respectively, while

TABLE VII. Bulk modulus, shear modulus, and Poisson ratio of hexagonal structure semiconductors. "N/A"= Not available for that source. Units: B and G in GPa.

Comp.	$B^{\rm exp}$	$B^{\rm AEL}_{\rm VRH}$	$B^{\rm MP}_{\rm VRH}$	$B^{\rm AGL}_{\rm Static}$	$B^{\rm BM}_{\rm Static}$	$B^{\rm Vinet}_{\rm Static}$	$B^{\rm BCN}_{\rm Static}$	$G^{\rm exp}$	$G^{\rm AEL}_{\rm Voigt}$	$G^{\rm AEL}_{\rm Reuss}$	$G^{\rm AEL}_{\rm VRH}$	$G^{\rm MP}_{\rm VRH}$	$\sigma^{\rm exp}$	$\sigma^{\rm AEL}$	$\sigma^{\rm MP}$
SiC	219 [105]	213	213	204	208	207	207	198 [105]	188	182	185	187	0.153 [105]	0.163	0.16
AlN	211 [90,106]	195	194	187	190	189	189	135 [90,106]	123	122	122	122	0.237 [90,106]	0.241	0.24
	200 [107]							130 [107]					0.234 [107]		
GaN	195 [66,108]	175	172	166	167	166	168	51.6 [66,108]	107	105	106	105	0.378 [66,108]	0.248	0.25
	210 [109]							123 [109]					0.255 [109]		
ZnO	143 [66,110]	137	130	128	129	127	129	49.4 [66,110]	51.7	51.0	51.4	41.2	0.345 [66,110]	0.334	0.36
BeO	224.4 [111]	206	208	195	195	192	198	168 [111]	157	154	156	156	0.201 [111]	0.198	0.2
CdS	60.7 [66,110]	55.4	53.3	49.7	50.3	49.4	50.6	18.2 [66,110]	17.6	17.0	17.3	17.6	0.364 [66,110]	0.358	0.35
InSe	37.1 [112]	19.2	N/A	39.8	40.8	39.7	41.0	14.8 [112]	14.9	12.3	13.6	N/A	0.324 [112]	0.214	N/A
InN	126 [113]	124	N/A	118	120	119	119	N/A	55.4	54.4	54.9	N/A	N/A	0.308	N/A

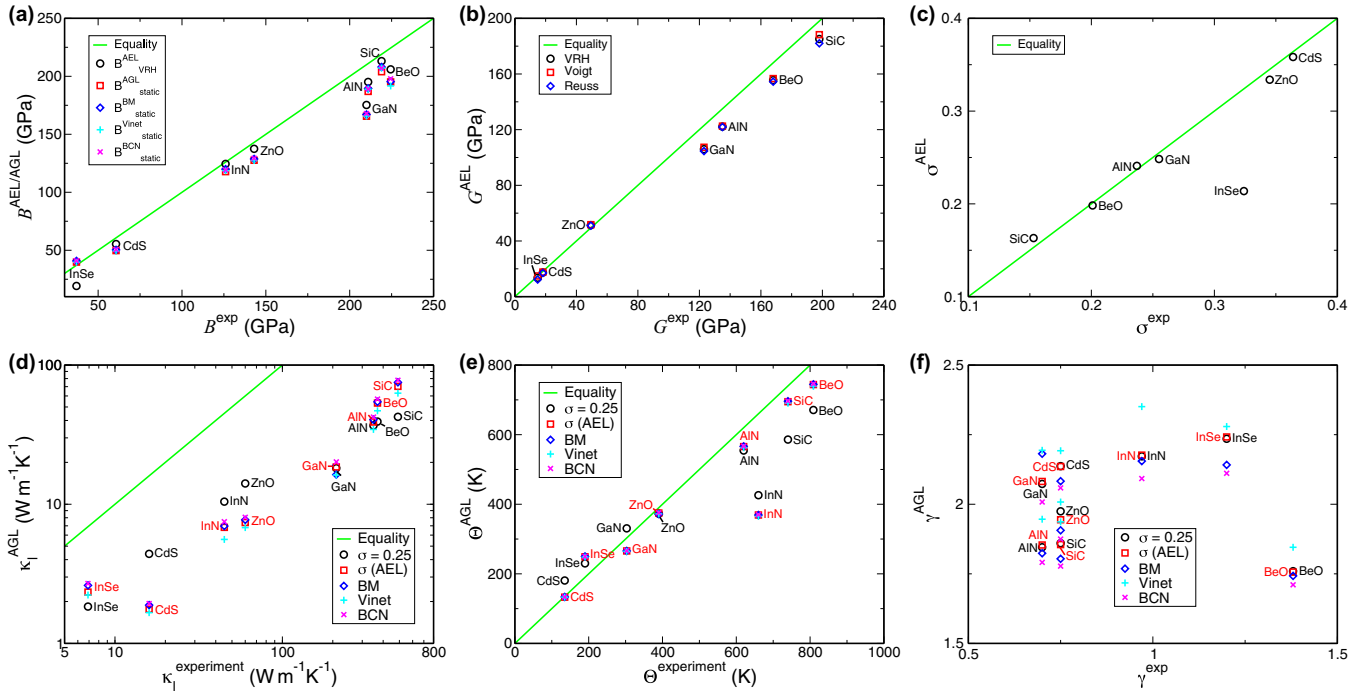

FIG. 3. (a) Bulk modulus, (b) shear modulus, (c) Poisson ratio, (d) lattice thermal conductivity, (e) Debye temperature, and (f) Grüneisen parameter of hexagonal structure semiconductors. The Debye temperatures plotted in (e) are θ_a, except for InSe and InN where θ_D values are quoted in Refs. [88,89,114].

the respective Spearman correlations were 0.943, 1.0, and 1.0, and the RMSrD values were 0.100, 0.091, and 0.036. These correlation values are very similar, and the general close agreement for the results for the values of B^{AEL}_{VRH}, G^{AEL}_{VRH}, and σ^{AEL} with those of B^{MP}_{VRH}, G^{MP}_{VRH}, and σ^{MP} demonstrate that the small differences in the parameters used for the DFT calculations make little difference to the results, indicating that the parameter set used here is robust for high-throughput calculations.

The thermal properties calculated using AGL are compared to the experimental values in Table VIII and are also plotted in Fig. 3. For the Debye temperature, the θ^{exp} values taken from Ref. [54] are for θ_a, and are mostly in good agreement with the calculated θ_a^{AGL} values. As in the case of the other

TABLE VIII. Lattice thermal conductivity, Debye temperature, and Grüneisen parameter of hexagonal structure semiconductors, comparing the effect of using the calculated value of the Poisson ratio to the previous approximation of $\sigma = 0.25$. The values listed for θ^{exp} are θ_a, except 190 K for InSe [88] and 660 K for InN [89,114], which are θ_D. "N/A" = Not available for that source. Units: κ in W m^{-1} K^{-1} and θ in Kelvin.

Comp.	κ^{exp}	κ^{AGL} ($\sigma = 0.25$) [34]	κ^{AGL}	θ^{exp}	θ_D^{AGL} (θ_a^{AGL}) ($\sigma = 0.25$) [34]	θ_D^{AGL} (θ_a^{AGL})	θ_D^{AEL}	γ^{exp}	γ^{AGL} ($\sigma = 0.25$) [34]	γ^{AGL}
SiC	490 [54]	42.49	70.36	740 [54]	930 (586)	1103 (695)	1138	0.75 [54]	1.86	1.86
AlN	350 [54]	36.73	39.0	620 [54]	880 (554)	898 (566)	917	0.7 [54]	1.85	1.85
GaN	210 [54]	18.17	18.54	390 [54]	592 (373)	595 (375)	606	0.7 [54]	2.07	2.08
ZnO	60 [54]	14.10	7.39	303 [54]	525 (331)	422 (266)	427	0.75 [54]	1.97	1.94
BeO	370 [54]	39.26	53.36	809 [54]	1065 (671)	1181 (744)	1235	1.38 [54,111,115]	1.76	1.76
CdS	16 [54]	4.40	1.76	135 [54]	287 (181)	211 (133)	213	0.75 [54]	2.14	2.14
InSe	6.9 [88]	1.84	2.34	190 [88]	230 (115)	249 (125)	168	1.2 [88]	2.24	2.24
InN	45 [89,114]	10.44	6.82	660 [89,114]	426 (268)	369 (232)	370	0.97 [114]	2.17	2.18

TABLE IX. Correlations between experimental values and AEL and AGL results for elastic and thermal properties for hexagonal structure semiconductors.

Property	Pearson (Linear)	Spearman (Rank Order)	RMSrD
$\kappa^{\rm exp}$ versus $\kappa^{\rm AGL}$ ($\sigma = 0.25$) [34]	0.977	1.0	0.887
$\kappa^{\rm exp}$ versus $\kappa^{\rm AGL}$	0.980	0.976	0.911
$\kappa^{\rm exp}$ versus $\kappa^{\rm BM}$	0.974	0.976	0.904
$\kappa^{\rm exp}$ versus $\kappa^{\rm Vinet}$	0.980	0.976	0.926
$\kappa^{\rm exp}$ versus $\kappa^{\rm BCN}$	0.980	0.976	0.895
$\theta^{\rm exp}$ versus $\theta^{\rm AGL}$ ($\sigma = 0.25$) [34]	0.960	0.976	0.233
$\theta^{\rm exp}$ versus $\theta^{\rm AGL}$	0.921	0.929	0.216
$\theta^{\rm exp}$ versus $\theta^{\rm BM}$	0.921	0.929	0.217
$\theta^{\rm exp}$ versus $\theta^{\rm Vinet}$	0.920	0.929	0.218
$\theta^{\rm exp}$ versus $\theta^{\rm BCN}$	0.921	0.929	0.216
$\gamma^{\rm exp}$ versus $\gamma^{\rm AGL}$ ($\sigma = 0.25$) [34]	−0.039	0.160	1.566
$\gamma^{\rm exp}$ versus $\gamma^{\rm AGL}$	−0.029	0.160	1.563
$\gamma^{\rm exp}$ versus $\gamma^{\rm BM}$	−0.124	−0.233	1.547
$\gamma^{\rm exp}$ versus $\gamma^{\rm Vinet}$	−0.043	0.012	1.677
$\gamma^{\rm exp}$ versus $\gamma^{\rm BCN}$	−0.054	0.098	1.467
$B^{\rm exp}$ versus $B^{\rm AEL}_{\rm VRH}$	0.990	0.976	0.201
$B^{\rm exp}$ versus $B^{\rm AGL}_{\rm Static}$	0.990	0.976	0.138
$B^{\rm exp}$ versus $B^{\rm BM}_{\rm Static}$	0.988	0.976	0.133
$B^{\rm exp}$ versus $B^{\rm Vinet}_{\rm Static}$	0.988	0.976	0.139
$B^{\rm exp}$ versus $B^{\rm BCN}_{\rm Static}$	0.990	0.976	0.130
$G^{\rm exp}$ versus $G^{\rm AEL}_{\rm VRH}$	0.998	1.0	0.090
$G^{\rm exp}$ versus $G^{\rm AEL}_{\rm Voigt}$	0.998	1.0	0.076
$G^{\rm exp}$ versus $G^{\rm AEL}_{\rm Reuss}$	0.998	1.0	0.115
$\sigma^{\rm exp}$ versus $\sigma^{\rm AEL}$	0.851	0.893	0.143

materials sets, the values obtained using the numerical $E(V)$ fit and the three different equations of state are very similar to each other, whereas $\theta_{\rm D}^{\rm AGL}$ calculated using $\sigma = 0.25$ differs significantly. In fact, the values of $\theta_{\rm D}^{\rm AGL}$ calculated with $\sigma^{\rm AEL}$ have a lower correlation with $\theta^{\rm exp}$ than the values calculated with $\sigma = 0.25$, although the RMSrD values are lower when $\sigma^{\rm AEL}$ is used. However, most of this discrepancy appears to be due to the clear outlier value for the material InN. When the values for this material are removed from the data set, the Pearson correlation values become very similar when both the $\sigma = 0.25$ and $\sigma = \sigma^{\rm AEL}$ values are used, increasing to 0.995 and 0.994, respectively.

The experimental and calculated values of the Grüneisen parameter are listed in Table VIII and in Ref. [65], and are plotted in Fig. 3(f). Again, the Debye model does not reproduce the experimental data, as the calculated values are often 2 to 3 times too large and the RMSrD is larger than 1.5. The corresponding correlations, shown in Table IX, are also quite poor, with no value higher than 0.160 for the Spearman correlations, and negative values for the Pearson correlations.

The comparison between the experimental thermal conductivity $\kappa^{\rm exp}$ and the calculated values is also quite poor [Fig. 3(d) and Table VIII], with RMSrD values of the order of 0.9. Considerable disagreements also exist between different experimental reports for most materials. Nevertheless, the Pearson correlations between the AGL calculated thermal conductivity values and the experimental values are high, ranging from 0.974 to 0.980, while the Spearman correlations are even higher, ranging from 0.976 to 1.0.

As for the rock-salt and zinc-blende material sets, Ref. [54] (Table 2.3) includes values of the thermal conductivity at 300 K for wurzite structure materials, calculated using the experimental values of the Debye temperature and Grüneisen parameter in the Leibfried-Schlömann equation. The Pearson and Spearman correlations are 0.996 and 1.0, respectively, which are slightly higher than the correlations obtained using the AGL calculated quantities. The difference is insignificant since all of these correlations are very high and could reliably serve as a screening tool of the thermal conductivity. However, as we noted in our previous work on AGL [34], the high correlations calculated with the experimental $\theta_{\rm a}$ and γ were obtained using $\gamma = 0.75$ for BeO. Table 2.3 of Ref. [54] also cites an alternative value of $\gamma = 1.38$ for BeO (Table VIII). Using this outlier value would severely degrade the results down to 0.7, for the Pearson correlation, and 0.829, for the Spearman correlation. These values are too low for a reliable screening tool. This demonstrates the ability of the AEL-AGL calculations to compensate for anomalies in the experimental data when they exist and still provide a reliable screening method for the thermal conductivity.

D. Rhombohedral materials

The elastic properties of a few materials with rhombohedral structures (space groups: $R\bar{3}mR$, No. 166, $R\bar{3}mH$, No. 166; Pearson symbol: hR5; AFLOW prototype: A2B3_hR5_166_c_ac [62,116]; and space group: $R\bar{3}cH$, No. 167; Pearson symbol: hR10; AFLOW prototype: A2B3_hR10_167_c_e [62,117]) are shown in Table X (we have left out the material Fe_2O_3, which was included in the data set in Table IV of Ref. [34], due to convergence issues with some of the strained structures required for the calculation of the elastic tensor). The comparison between experiment and calculation is qualitatively reasonable, but the scarcity of experimental results does not allow for a proper correlation analysis.

TABLE X. Bulk modulus, shear modulus, and Poisson ratio of rhombohedral semiconductors. "N/A" = Not available for that source. Units: B and G in GPa.

Comp.	$B^{\rm exp}$	$B^{\rm AEL}_{\rm VRH}$	$B^{\rm MP}_{\rm VRH}$	$B^{\rm AGL}_{\rm Static}$	$B^{\rm BM}_{\rm Static}$	$B^{\rm Vinet}_{\rm Static}$	$B^{\rm BCN}_{\rm Static}$	$G^{\rm exp}$	$G^{\rm AEL}_{\rm Voigt}$	$G^{\rm AEL}_{\rm Reuss}$	$G^{\rm AEL}_{\rm VRH}$	$G^{\rm MP}_{\rm VRH}$	$\sigma^{\rm exp}$	$\sigma^{\rm AEL}$	$\sigma^{\rm MP}$
Bi_2Te_3	37.0 [66,118]	28.8	15.0	43.7	44.4	43.3	44.5	22.4 [66,118]	23.5	16.3	19.9	10.9	0.248 [66,118]	0.219	0.21
Sb_2Te_3	N/A	22.9	N/A	45.3	46.0	45.2	46.0	N/A	20.6	14.5	17.6	N/A	N/A	0.195	N/A
Al_2O_3	254 [119]	231	232	222	225	224	224	163.1 [119]	149	144	147	147	0.235 [119]	0.238	0.24
Cr_2O_3	234 [120]	203	203	198	202	201	201	129 [120]	115	112	113	113	0.266 [120]	0.265	0.27
Bi_2Se_3	N/A	93.9	N/A	57.0	57.5	56.4	57.9	N/A	53.7	28.0	40.9	N/A	N/A	0.310	N/A

TABLE XI. Lattice thermal conductivity, Debye temperatures, and Grüneisen parameter of rhombohedral semiconductors, comparing the effect of using the calculated value of the Poisson ratio to previous approximation of $\sigma = 0.25$. The experimental Debye temperatures are θ_D for Bi_2Te_3 and Sb_2Te_3, and θ_a for Al_2O_3. "N/A" = Not available for that source. Units: κ in W m^{-1} K^{-1} and θ in Kelvin.

Comp.	κ^{exp}	κ^{AGL} ($\sigma = 0.25$) [34]	κ^{AGL}	θ^{exp}	θ_D^{AGL} (θ_a^{AGL}) ($\sigma = 0.25$) [34]	θ_D^{AGL} (θ_a^{AGL})	θ_D^{AEL}	γ^{exp}	γ^{AGL} ($\sigma = 0.25$) [34]	γ^{AGL}
Bi_2Te_3	1.6 [88]	2.79	3.35	155 [88]	191 (112)	204 (119)	161	1.49 [88]	2.13	2.14
Sb_2Te_3	2.4 [88]	2.90	4.46	160 [88]	217 (127)	243 (142)	170	1.49 [88]	2.2	2.11
Al_2O_3	30 [121]	20.21	21.92	390 [53]	927 (430)	952 (442)	975	1.32 [53]	1.91	1.91
Cr_2O_3	16 [90,122]	10.87	12.03	N/A	733 (340)	717 (333)	720	N/A	2.26	2.10
Bi_2Se_3	1.34 [90]	3.60	2.41	N/A	223 (130)	199 (116)	241	N/A	2.08	2.12

The thermal properties calculated using AGL are compared to the experimental values in Table XI and the thermal conductivity is also plotted in Fig. 4(a). The experimental Debye temperatures are θ_D for Bi_2Te_3 and Sb_2Te_3, and θ_a for Al_2O_3. The values obtained using the numerical $E(V)$ fit and the three different equations of state (see Ref. [65]) are very similar, but just roughly reproduce the experiments.

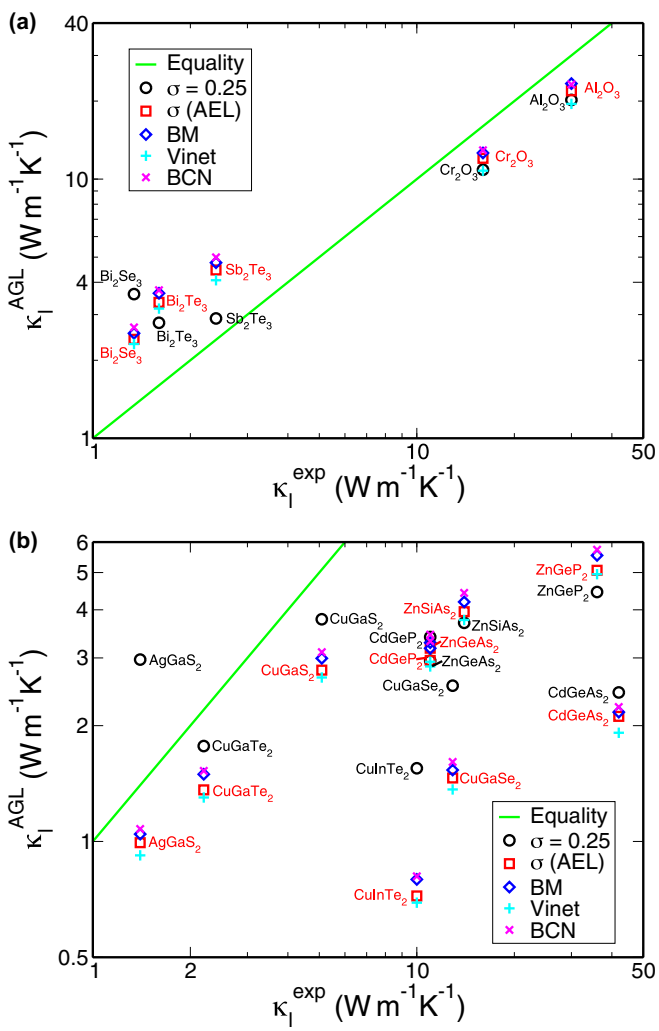

FIG. 4. (a) Lattice thermal conductivity of rhombohedral semiconductors at 300 K. (b) Lattice thermal conductivity of body-centred tetragonal semiconductors at 300 K.

The calculated Grüneisen parameters are about 50% larger than the experimental ones, and the value of σ used makes little difference in the calculation. The absolute agreement between the AGL values and κ^{exp} is also quite poor [Fig. 4(a)]. However, despite all these discrepancies, the Pearson correlations between the calculated thermal conductivities and the experimental values are all high, of the order of 0.998, while the Spearman correlations range from 0.7 to 1.0, with all of the different equations of state having very similar correlations with experiment, as shown in Table XII. Using the calculated σ^{AEL}, versus the rough Cauchy approximation, improves the Spearman correlation from 0.7 to 1.0.

E. Body-centred tetragonal materials

The mechanical properties of the body-centred tetragonal materials (space group: $I\bar{4}2d$, No. 122; Pearson symbol: tI16; AFLOW prototype: ABC2_tI16_122_a_b_d [62,123]) of Table V of Ref. [34] are reported in Table XIII. The calculated bulk moduli miss considerably the few available experimental results, while the shear moduli are well reproduced. Reasonable estimates are also obtained for the Poisson ratio.

The thermal properties are reported in Table XIV and Fig. 4(b). The θ^{exp} values are all for θ_D, and in most cases are in good agreement with the values obtained with the AEL

TABLE XII. Correlations between experimental values and AEL and AGL results for elastic and thermal properties for rhombohedral structure semiconductors.

Property	Pearson (Linear)	Spearman (Rank Order)	RMSrD
κ^{exp} versus κ^{AGL} ($\sigma = 0.25$) [34]	0.997	0.7	0.955
κ^{exp} versus κ^{AGL}	0.998	1.0	0.821
κ^{exp} versus κ^{BM}	0.997	1.0	0.931
κ^{exp} versus κ^{Vinet}	0.998	1.0	0.741
κ^{exp} versus κ^{BCN}	0.997	1.0	1.002

TABLE XIII. Bulk modulus, shear modulus and Poisson ratio of body-centred tetragonal semiconductors. Note that there appears to be an error in Table 1 of Ref. [124] where the bulk modulus values are stated to be in units of 10^{12} Pa. This seems unlikely, as that would give a bulk modulus for $CuInTe_2$ an order of magnitude larger than that for diamond. Also, units of 10^{12} Pa would be inconsistent with the experimental results listed in Ref. [125], so therefore it seems that these values are in units of 10^{10} Pa, which are the values shown here. "N/A" = Not available for that source. Units: B and G in GPa.

Comp.	B^{exp}	$B^{\mathrm{AEL}}_{\mathrm{VRH}}$	$B^{\mathrm{MP}}_{\mathrm{VRH}}$	$B^{\mathrm{AGL}}_{\mathrm{Static}}$	$B^{\mathrm{BM}}_{\mathrm{Static}}$	$B^{\mathrm{Vinet}}_{\mathrm{Static}}$	$B^{\mathrm{BCN}}_{\mathrm{Static}}$	G^{exp}	$G^{\mathrm{AEL}}_{\mathrm{Voigt}}$	$G^{\mathrm{AEL}}_{\mathrm{Reuss}}$	$G^{\mathrm{AEL}}_{\mathrm{VRH}}$	$G^{\mathrm{MP}}_{\mathrm{VRH}}$	σ^{exp}	σ^{AEL}	σ^{MP}
$CuGaTe_2$	N/A	47.0	N/A	42.5	43.2	42.0	43.5	N/A	25.1	22.1	23.6	N/A	N/A	0.285	N/A
$ZnGeP_2$	N/A	73.1	74.9	70.1	71.1	70.0	71.4	N/A	50.5	46.2	48.4	48.9	N/A	0.229	0.23
$ZnSiAs_2$	N/A	67.4	65.9	63.4	64.3	63.1	64.6	N/A	44.4	40.4	42.4	42.2	N/A	0.240	0.24
$CuInTe_2$	36.0 [125] 45.4 [124]	53.9	N/A	38.6	39.2	38.2	39.4	N/A	20.4	17.2	18.8	N/A	0.313 [124]	0.344	N/A
$AgGaS_2$	67.0 [126]	70.3	N/A	56.2	57.1	56.0	57.4	20.8 [126]	20.7	17.4	19.1	N/A	0.359 [126]	0.375	N/A
$CdGeP_2$	N/A	65.3	65.2	60.7	61.6	60.4	61.9	N/A	37.7	33.3	35.5	35.0	N/A	0.270	0.27
$CdGeAs_2$	69.9 [127]	52.6	N/A	49.2	49.6	48.3	49.9	29.5 [127]	30.9	26.2	28.6	N/A	0.315 [127]	0.270	N/A
$CuGaS_2$	94.0 [128]	73.3	N/A	69.0	69.9	68.7	70.6	N/A	37.8	32.4	35.1	N/A	N/A	0.293	N/A
$CuGaSe_2$	N/A	69.9	N/A	54.9	55.6	54.4	56.0	N/A	30.3	26.0	28.1	N/A	N/A	0.322	N/A
$ZnGeAs_2$	N/A	59.0	N/A	56.2	56.7	55.5	57.1	N/A	39.0	35.6	37.3	N/A	N/A	0.239	N/A

calculated σ. The values from the numerical $E(V)$ fit and the three different equations of state are again very similar, but differ significantly from $\theta_{\mathrm{D}}^{\mathrm{AGL}}$ calculated with $\sigma = 0.25$.

The comparison of the experimental thermal conductivity κ^{exp} to the calculated values, in Fig. 4(b), shows poor reproducibility. The available data can thus only be considered a rough indication of their order of magnitude. The Pearson and Spearman correlations are listed in Table XV and are also quite low for all types of calculation, but somewhat better when the calculated σ^{AEL} is used instead of the Cauchy approximation.

F. Miscellaneous materials

In this section, we consider materials with various other structures, as in Table VI of Ref. [34]: $CoSb_3$ and $IrSb_3$ (space group: $Im\bar{3}$, No. 204; Pearson symbol: cI32; AFLOW prototype: A3B_cI32_204_g_c [62,136]), ZnSb ($Pbca$, No. 61; oP16; AFLOW prototype: AB_oP16_61_c_c [62,137]), Sb_2O_3 ($Pccn$, No. 56; oP20), InTe ($Pm\bar{3}m$, No. 221; cP2; AFLOW prototype: AB_cP2_221_b_a [62,138], and $I4/mcm$, No. 140; tI16), Bi_2O_3 ($P121/c1$, No. 14; mP20), and SnO_2 ($P42/mnm$, No. 136; tP6; A2B_tP6_136_f_a [62,139]). Two

TABLE XIV. Lattice thermal conductivity at 300 K, Debye temperatures and Grüneisen parameter of body-centred tetragonal semiconductors, comparing the effect of using the calculated value of the Poisson ratio to previous approximation of $\sigma = 0.25$. "N/A" = Not available for that source. Units: κ in W m^{-1} K^{-1} and θ in Kelvin.

Comp.	κ^{exp}	κ^{AGL} ($\sigma = 0.25$) [34]	κ^{AGL}	θ^{exp}	$\theta_{\mathrm{D}}^{\mathrm{AGL}}$ ($\theta_{\mathrm{a}}^{\mathrm{AGL}}$) ($\sigma = 0.25$) [34]	$\theta_{\mathrm{D}}^{\mathrm{AGL}}$ ($\theta_{\mathrm{a}}^{\mathrm{AGL}}$)	$\theta_{\mathrm{D}}^{\mathrm{AEL}}$	γ^{exp}	γ^{AGL} ($\sigma = 0.25$) [34]	γ^{AGL}
$CuGaTe_2$	2.2 [88]	1.77	1.36	226 [88]	234 (117)	215 (108)	218	1.46 [88]	2.32	2.32
$ZnGeP_2$	35 [90,129] 36 [90,129] 18 [90,131,132]	4.45	5.07	500 [90] 428 [130]	390 (195)	408 (204)	411	N/A	2.13	2.14
$ZnSiAs_2$	14 [90,131,132]	3.70	3.96	347 [90,133]	342 (171)	350 (175)	354	N/A	2.15	2.15
$CuInTe_2$	10 [90,134]	1.55	0.722	185 [90,134] 195 [90,135]	215 (108)	166 (83)	185	0.93 [134]	2.33	2.32
$AgGaS_2$	1.4 [90,129]	2.97	0.993	255 [90,130]	324 (162)	224 (112)	237	N/A	2.20	2.20
$CdGeP_2$	11 [90,131,132]	3.40	2.96	340 [90,130]	335 (168)	320 (160)	324	N/A	2.20	2.21
$CdGeAs_2$	42 [90,131]	2.44	2.11	241 [133]	266 (133)	254 (127)	255	N/A	2.20	2.20
$CuGaS_2$	5.09 [90]	3.78	2.79	356 [90,130]	387 (194)	349 (175)	349	N/A	2.24	2.24
$CuGaSe_2$	12.9 [90,134]	2.54	1.46	262 [90,135]	294 (147)	244 (122)	265	N/A	2.27	2.26
$ZnGeAs_2$	11 [90,131]	2.95	3.18	N/A	299 (150)	307 (154)	308	N/A	2.16	2.17

TABLE XV. Correlations between experimental values and AEL and AGL results for elastic and thermal properties for body-centred tetragonal structure semiconductors.

Property	Pearson (Linear)	Spearman (Rank Order)	RMSrD
κ^{exp} versus κ^{AGL} ($\sigma = 0.25$) [34]	0.265	0.201	0.812
κ^{exp} versus κ^{AGL}	0.472	0.608	0.766
κ^{exp} versus κ^{BM}	0.467	0.608	0.750
κ^{exp} versus κ^{Vinet}	0.464	0.608	0.778
κ^{exp} versus κ^{BCN}	0.460	0.608	0.741

different structures are listed for InTe. In Ref. [34], we considered its simple cubic structure, but this is a high-pressure phase [140], while the ambient pressure phase is body-centred tetragonal. It appears that the thermal conductivity results should be for the body-centred tetragonal phase [91], therefore both sets of results are reported here. The correlation values shown in the tables below were calculated for the body-centred tetragonal structure.

The elastic properties are shown in Table XVI. Large discrepancies appear between the results of all calculations and the few available experimental results.

The thermal properties are compared to the experimental values in Table XVII. The experimental Debye temperatures are for θ_D, except ZnSb for which it is θ_a. Good agreement is found between calculation and the few available experimental values. Again, the numerical $E(V)$ fit and the three different equations of state give similar results. For the Grüneisen parameter, experiment and calculations again differ considerably, while the changes due to the different values of σ used in the calculations are negligible.

The experimental thermal conductivity κ^{exp} is compared in Table XVII to the thermal conductivity calculated with AGL using the Leibfried-Schlömann equation (37) for κ^{AGL}, while the values obtained for κ^{BM},κ^{Vinet} and κ^{BCN} are listed in Ref. [65]. The absolute agreement between the AGL values and κ^{exp} is quite poor. The scarcity of experimental data from different sources on the thermal properties of these materials prevents reaching definite conclusions regarding the true values of these properties. The available data can thus only be considered as a rough indication of their order of magnitude.

For these materials, the Pearson correlation between the calculated and experimental values of the thermal conductivity ranges from 0.438 to 0.937, while the corresponding Spearman correlations range from −0.143 to 0.071, as shown in Table XVIII. In this case, using σ^{AEL} in the AGL calculations does not improve the correlations, instead actually it is lowering the values somewhat. However, it should be noted that the Pearson correlation is heavily influenced by the values for SnO_2. When this entry is removed from the list, the Pearson correlation values fall to −0.105 and −0.275 when the $\sigma = 0.25$ and $\sigma = \sigma^{AEL}$ values are used, respectively. The low correlation values, particularly for the Spearman correlation, for this set of materials demonstrates the importance of the information about the material structure when interpreting results obtained using the AGL method in order to identify candidate materials for specific thermal applications. This is partly due to the fact that the Grüneisen parameter values tend to be similar for materials with the same structure. Therefore the effect of the Grüneisen parameter on the ordinal ranking of the lattice thermal conductivity of materials with the same structure is small.

G. Thermomechanical properties from LDA

The thermomechanical properties of a randomly selected subset of the materials investigated in this work were calculated using LDA in order to check the impact of the choice of exchange-correlation functional on the results. For the LDA calculations, all structures were first re-relaxed using the LDA exchange-correlation functional with VASP using the appropriate parameters and potentials as described in the AFLOW standard [37], and then the appropriate strained structures were calculated using LDA. These calculations were restricted to a subset of materials to limit the total number of additional first-principles calculations required, and the materials were selected randomly from each of the sets in the previous sections so as to cover as wide a range of different structure types as possible, given the available experimental data. Results for elastic properties obtained using LDA, GGA, and experimental measurements are shown in Table XIX, while the thermal properties are shown in Table XX. All thermal properties listed in Table XX were calculated using σ^{AEL} in the expression for the Debye temperature.

In general, the LDA values for elastic and thermal properties are slightly higher than the GGA values, as would be generally expected due to their relative tendencies to overbind and underbind, respectively [144,145]. The correlations and RMSrD of both the LDA and GGA results with experiment for this set of materials are listed in Table XXI. The Pearson

TABLE XVI. Bulk modulus, shear modulus, and Poisson ratio of materials with various structures. "N/A" = Not available for that source. Units: B and G in GPa.

Comp.	Pearson	B^{exp}	B^{AEL}_{VRH}	B^{MP}_{VRH}	B^{AGL}_{Static}	B^{BM}_{Static}	B^{Vinet}_{Static}	B^{BCN}_{Static}	G^{exp}	G^{AEL}_{Voigt}	G^{AEL}_{Reuss}	G^{AEL}_{VRH}	G^{MP}_{VRH}	σ^{exp}	σ^{AEL}	σ^{MP}
$CoSb_3$	cI32	N/A	78.6	82.9	75.6	76.1	75.1	76.3	N/A	57.2	55.1	56.2	57.0	N/A	0.211	0.22
$IrSb_3$	cI32	N/A	97.5	98.7	94.3	94.8	93.8	95.5	N/A	60.9	59.4	60.1	59.7	N/A	0.244	0.25
ZnSb	oP16	N/A	47.7	47.8	46.7	47.0	46.0	47.7	N/A	29.2	27.0	28.1	28.2	N/A	0.253	0.25
Sb_2O_3	oP20	N/A	16.5	19.1	97.8	98.7	97.8	98.7	N/A	22.8	16.4	19.6	20.4	N/A	0.0749	0.11
InTe	cP2	90.2 [140]	41.7	N/A	34.9	34.4	33.6	34.7	N/A	8.41	8.31	8.36	N/A	N/A	0.406	N/A
InTe	tI16	46.5 [140]	20.9	N/A	32.3	33.1	32.2	33.2	N/A	13.4	13.0	13.2	N/A	N/A	0.239	N/A
Bi_2O_3	mP20	N/A	48.0	54.5	108	110	109	109	N/A	30.3	25.9	28.1	29.9	N/A	0.255	0.27
SnO_2	tP6	212 [141]	159	N/A	158	162	161	161	106 [141]	86.7	65.7	76.2	N/A	0.285 [141]	0.293	N/A

TABLE XVII. Lattice thermal conductivity at 300 K, Debye temperatures, and Grüneisen parameter of materials with various structures, comparing the effect of using the calculated value of the Poisson ratio to the previous approximation of $\sigma = 0.25$. The experimental Debye temperatures are θ_D, except ZnSb for which it is θ_a. "N/A" = Not available for that source. Units: κ in W m^{-1} K^{-1} and θ in Kelvin.

Comp.	Pearson	κ^{exp}	κ^{AGL} ($\sigma = 0.25$) [34]	κ^{AGL}	θ^{exp}	θ_D^{AGL} (θ_a^{AGL}) ($\sigma = 0.25$) [34]	θ_D^{AGL} (θ_a^{AGL})	θ_D^{AEL}	γ^{exp}	γ^{AGL} ($\sigma = 0.25$) [34]	γ^{AGL}
$CoSb_3$	cI32	10 [88]	1.60	2.60	307 [88]	284 (113)	310 (123)	312	0.95 [88]	2.63	2.33
$IrSb_3$	cI32	16 [88]	2.64	2.73	308 [88]	283 (112)	286 (113)	286	1.42 [88]	2.34	2.34
ZnSb	oP16	3.5 [55,142]	1.24	1.23	92 [55]	244 (97)	242 (96)	237	0.76 [55,142]	2.24	2.23
Sb_2O_3	oP20	0.4 [90]	3.45	8.74	N/A	418 (154)	572 (211)	238	N/A	2.13	2.12
InTe	cP2	N/A	3.12	0.709	N/A	191 (152)	113 (90)	116	N/A	2.28	2.19
InTe	tP16	1.7 [88,91]	1.32	1.40	186 [88]	189 (95)	193 (97)	150	1.0 [88]	2.23	2.24
Bi_2O_3	mP20	0.8 [90]	3.04	2.98	N/A	345 (127)	342 (126)	223	N/A	2.10	2.10
SnO_2	tP6	98 [143] 55 [143]	9.56	6.98	N/A	541 (298)	487 (268)	480	N/A	2.48	2.42

and Spearman correlation values for LDA and GGA are very close to each other for most of the listed properties. The RMSrD values show greater differences, although it isn't clear that one of the exchange-correlation functionals consistently gives better predictions than the other. Therefore the choice of exchange-correlation functional will make little difference to the predictive capability of the workflow, so we choose to use GGA-PBE as it is the functional used for performing the structural relaxation for the entries in the AFLOW data repository.

H. AGL predictions for thermal conductivity

The AEL-AGL methodology has been applied for high-throughput screening of the elastic and thermal properties of over 3000 materials included in the AFLOW database [36]. Tables XXII and XXIII list those found to have the highest and lowest thermal conductivities, respectively. The high-conductivity list is unsurprisingly dominated by various phases of elemental carbon, boron nitride, boron carbide and boron carbon nitride, while all other high-conductivity materials also contain at least one of the elements C, B, or N.

TABLE XVIII. Correlations between experimental values and AEL and AGL results for elastic and thermal properties for materials with miscellaneous structures.

Property	Pearson (Linear)	Spearman (Rank Order)	RMSrD
κ^{exp} versus κ^{AGL} ($\sigma = 0.25$) [34]	0.937	0.071	3.38
κ^{exp} versus κ^{AGL}	0.438	−0.143	8.61
κ^{exp} versus κ^{BM}	0.498	−0.143	8.81
κ^{exp} versus κ^{Vinet}	0.445	0.0	8.01
κ^{exp} versus κ^{BCN}	0.525	−0.143	9.08

The low thermal conductivity list tends to contain materials with large unit cells and heavier elements such as Hg, Tl, Pb, and Au.

By combining the AFLOW search for thermal conductivity values with other properties such as chemical, electronic or structural factors, candidate materials for specific engineering applications can be rapidly identified for further in-depth analysis using more accurate computational methods and for experimental examination. The full set of thermomechanical properties calculated using AEL-AGL for over 3500 entries can be accessed online at aflow.org [146], which incorporates search and sort functionality to generate customized lists of materials.

IV. CONCLUSIONS

We have implemented the "Automatic Elasticity Library" framework for *ab-initio* elastic constant calculations, and integrated it with the "Automatic GIBBS Library" implementation of the GIBBS quasiharmonic Debye model within the AFLOW and Materials Project frameworks. We used it to automatically calculate the bulk modulus, shear modulus, Poisson ratio, thermal conductivity, Debye temperature, and Grüneisen parameter of materials with various structures and compared them with available experimental results.

A major aim of high-throughput calculations is to identify useful property descriptors for screening large datasets of structures [31]. Here, we have examined whether the *inexpensive* Debye model, despite its well known deficiencies, can be usefully leveraged for estimating thermal properties of materials by analyzing correlations between calculated and corresponding experimental quantities.

It is found that the AEL calculation of the elastic moduli reproduces the experimental results quite well, within 5% to 20%, particularly for materials with cubic and hexagonal structures. The AGL method, using an isotropic approximation

TABLE XIX. Bulk modulus, shear modulus, and Poisson ratio of a subset of the materials investigated in this work, comparing the effect of using different exchange-correlation functionals. "N/A"= Not available for that source. Units: B and G in GPa.

Comp.	B^{exp}	$B^{\mathrm{GGA}}_{\mathrm{VRH}}$	$B^{\mathrm{LDA}}_{\mathrm{VRH}}$	$B^{\mathrm{GGA}}_{\mathrm{Static}}$	$B^{\mathrm{LDA}}_{\mathrm{Static}}$	G^{exp}	$G^{\mathrm{GGA}}_{\mathrm{Voigt}}$	$G^{\mathrm{LDA}}_{\mathrm{Voigt}}$	$G^{\mathrm{GGA}}_{\mathrm{Reuss}}$	$G^{\mathrm{LDA}}_{\mathrm{Reuss}}$	$G^{\mathrm{GGA}}_{\mathrm{VRH}}$	$G^{\mathrm{LDA}}_{\mathrm{VRH}}$	σ^{exp}	σ^{GGA}	σ^{LDA}
Si	97.8 [66,71]	89.1	96.9	84.2	92.1	66.5 [66,71]	64	65	61	61.9	62.5	63.4	0.223 [66,71]	0.216	0.231
BN	367.0 [67]	372	402	353	382	N/A	387	411	374	395	380	403	N/A	0.119	0.124
GaSb	57.0 [67]	47.0	58.3	41.6	52.3	34.2 [78]	30.8	35.3	28.3	32.2	29.6	33.7	0.248 [78]	0.240	0.258
InAs	60.0 [67]	50.1	62.3	45.7	57.4	29.5 [66,81]	27.3	30.1	24.2	26.4	25.7	28.2	0.282 [66,81]	0.281	0.303
ZnS	77.1 [67]	71.2	88.4	65.8	83.3	30.9 [66]	36.5	42.1	31.4	35.7	33.9	38.9	0.318 [66]	0.294	0.308
NaCl	25.1 [95]	24.9	33.3	20.0	27.6	14.6 [95]	14.0	19.8	12.9	16.6	13.5	18.2	0.255 [95]	0.271	0.269
KI	12.2 [95]	10.9	16.3	8.54	13.3	5.96 [95]	6.05	9.39	4.39	5.3	5.22	7.35	0.290 [95]	0.294	0.305
RbI	11.1 [95]	9.90	14.8	8.01	12.1	5.03 [95]	5.50	8.54	3.65	3.94	4.57	6.24	0.303 [95]	0.300	0.315
MgO	164 [97]	152	164	142	163	131 [97]	119	138	115	136	117	137	0.185 [97]	0.194	0.173
CaO	113 [98]	105	129	99.6	122	81.0 [98]	73.7	87.4	73.7	86.3	73.7	86.9	0.210 [98]	0.216	0.225
GaN	195 [66,108]	175	202	166	196	51.6 [66,108]	107	116	105	113	106	114	0.378 [66,108]	0.248	0.262
	210 [109]					123 [109]							0.255 [109]		
CdS	60.7 [66,110]	55.4	68.2	49.7	64.1	18.2 [66,110]	17.6	18.4	17.0	17.8	17.3	18.1	0.364 [66,110]	0.358	0.378
Al_2O_3	254 [119]	231	259	222	250	163.1 [119]	149	166	144	163	147	165	0.235 [119]	0.238	0.238
$CdGeP_2$	N/A	65.3	78.4	60.7	74.5	N/A	37.7	42.1	33.3	36.8	35.5	39.4	N/A	0.270	0.285
$CuGaSe_2$	N/A	69.9	76.4	54.9	72.1	N/A	30.3	34.7	26.0	30.0	28.1	32.3	N/A	0.322	0.315
$CoSb_3$	N/A	78.6	99.6	75.6	96.1	N/A	57.2	67.1	55.1	64.2	56.2	65.7	N/A	0.211	0.23

TABLE XX. Thermal properties lattice thermal conductivity at 300 K, Debye temperature, and Grüneisen parameter of a subset of materials, comparing the effect of using different exchange-correlation functionals. The values listed for θ^{exp} are θ_{a}, except 340 K for $CdGeP_2$ [90,130], 262 K for $CuGaSe_2$ [90,135], and 307 K for $CoSb_3$ [88] which are θ_{D}. Units: κ in W m^{-1} K^{-1} and θ in Kelvin.

Comp.	κ^{exp}	κ^{GGA}	κ^{LDA}	θ^{exp}	$\theta^{\mathrm{GGA}}_{\mathrm{D}}$ ($\theta^{\mathrm{GGA}}_{\mathrm{a}}$)	$\theta^{\mathrm{LDA}}_{\mathrm{D}}$ ($\theta^{\mathrm{LDA}}_{\mathrm{a}}$)	γ^{exp}	γ^{GGA}	γ^{LDA}
Si	166 [54]	26.19	27.23	395 [53,54]	610 (484)	614 (487)	1.06 [54] 0.56 [53]	2.06	2.03
BN	760 [54]	281.6	312.9	1200 [54]	1793 (1423)	1840 (1460)	0.7 [54]	1.75	1.72
GaSb	40 [54]	4.96	5.89	165 [53,54]	240 (190)	254 (202)	0.75 [53,54]	2.28	2.25
InAs	30 [54]	4.33	4.92	165 [53,54]	229 (182)	238 (189)	0.57 [53,54]	2.26	2.22
ZnS	27 [54]	8.38	9.58	230 [53,54]	341 (271)	363 (288)	0.75 [53,54]	2.00	2.02
NaCl	7.1 [54]	2.12	2.92	220 [53,54]	271 (215)	312 (248)	1.56 [53,54]	2.23	2.29
KI	2.6 [54]	0.525	0.811	87 [53,54]	116 (92)	137 (109)	1.45 [53,54]	2.35	2.37
RbI	2.3 [54]	0.368	0.593	84 [53,54]	97 (77)	115 (91)	1.41 [53,54]	2.47	2.45
MgO	60 [54]	44.5	58.4	600 [53,54]	849 (674)	935 (742)	1.44 [53,54]	1.96	1.95
CaO	27 [54]	24.3	28.5	450 [53,54]	620 (492)	665 (528)	1.57 [53,54]	2.06	2.09
GaN	210 [54]	18.54	21.34	390 [54]	595 (375)	619 (390)	0.7 [54]	2.08	2.04
CdS	16 [54]	1.76	1.84	135 [54]	211 (133)	217 (137)	0.75 [54]	2.14	2.14
Al_2O_3	30 [121]	21.92	25.36	390 [53]	952 (442)	1002 (465)	1.32 [53]	1.91	1.91
$CdGeP_2$	11 [90,131,132]	2.96	3.47	340 [90,130]	320 (160)	337 (169)	N/A	2.21	2.18
$CuGaSe_2$	12.9 [90,134]	1.46	2.23	262 [90,135]	244 (122)	281 (141)	N/A	2.26	2.23
$CoSb_3$	10 [88]	2.60	3.25	307 [88]	310 (123)	332 (132)	0.95 [88]	2.33	2.28

TABLE XXI. Correlations between experimental values and AEL and AGL results for elastic and thermal properties comparing the LDA and GGA exchange-correlation functionals.

Property	Pearson (Linear)	Spearman (Rank Order)	RMSrD
κ^{exp} versus κ^{GGA}	0.963	0.867	0.755
κ^{exp} versus κ^{LDA}	0.959	0.848	0.706
θ^{exp} versus θ^{GGA}	0.996	0.996	0.119
θ^{exp} versus θ^{LDA}	0.996	0.996	0.174
γ^{exp} versus γ^{GGA}	0.172	0.130	1.514
γ^{exp} versus γ^{LDA}	0.265	0.296	1.490
B^{exp} versus $B^{\text{GGA}}_{\text{VRH}}$	0.995	1.0	0.111
B^{exp} versus $B^{\text{LDA}}_{\text{VRH}}$	0.996	1.0	0.185
B^{exp} versus $B^{\text{GGA}}_{\text{Static}}$	0.996	1.0	0.205
B^{exp} versus $B^{\text{LDA}}_{\text{Static}}$	0.998	1.0	0.072
G^{exp} versus $G^{\text{GGA}}_{\text{VRH}}$	0.999	0.993	0.108
G^{exp} versus $G^{\text{LDA}}_{\text{VRH}}$	0.997	0.986	0.153
G^{exp} versus $G^{\text{GGA}}_{\text{Voigt}}$	0.998	0.993	0.096
G^{exp} versus $G^{\text{LDA}}_{\text{Voigt}}$	0.996	0.986	0.315
G^{exp} versus $G^{\text{GGA}}_{\text{Reuss}}$	0.999	0.993	0.163
G^{exp} versus $G^{\text{LDA}}_{\text{Reuss}}$	0.997	0.993	0.111
σ^{exp} versus σ^{GGA}	0.982	0.986	0.037
σ^{exp} versus σ^{LDA}	0.983	0.993	0.052

TABLE XXII. Materials from AFLOW database with the highest thermal conductivities as predicted using the AEL-AGL methodology. Units: κ in W m^{-1} K^{-1}.

Comp.	Pearson	Space group No.	κ^{AGL}
C	cF8	227	420
BN	cF8	216	282
C	hP4	194	272
C	tI8	139	206
BC_2N	oP4	25	188
BN	hP4	186	178
C	hP8	194	167
C	cI16	206	162
C	oS16	65	147
C	mS16	12	145
BC_7	tP8	115	145
BC_5	oI12	44	137
Be_2C	cF12	225	129
CN_2	tI6	119	127
C	hP12	194	127
BC_7	oP8	25	125
$B_2C_4N_2$	oP8	17	120
MnB_2	hP3	191	117
C	hP4	194	117
SiC	cF8	216	113
TiB_2	hP3	191	110
AlN	cF8	225	107
BP	cF8	216	105
C	hP16	194	105
VN	hP2	187	101

TABLE XXIII. Materials from AFLOW database with the lowest thermal conductivities as predicted using the AEL-AGL methodology. Units: κ in W m^{-1} K^{-1}.

Comp.	Pearson	Space group No.	κ^{AGL}
$Hg_{33}Rb_3$	cP36	221	0.0113
$Hg_{33}K_3$	cP36	221	0.0116
Cs_6Hg_{40}	cP46	223	0.0136
$Ca_{16}Hg_{36}$	cP52	215	0.0751
CrTe	cF8	216	0.081
Hg_4K_2	oI12	74	0.086
Sb_6Tl_{21}	cI54	229	0.089
Se	cF24	227	0.093
$Cs_8I_{24}Sn_4$	cF36	225	0.104
$Ag_2Cr_4Te_8$	cF56	227	0.107
AsCdLi	cF12	216	0.116
$Au_{36}In_{16}$	cP52	215	0.117
Cd_3In	cP4	221	0.128
AuLiSb	cF12	216	0.130
K_5Pb_{24}	cI58	217	0.135
K_8Sn_{46}	cP54	223	0.142
$Au_7Cd_{16}Na_6$	cF116	225	0.145
Cs	cI2	229	0.148
$Cs_8Pb_4Cl_{24}$	cF36	225	0.157
$Au_4In_8Na_{12}$	cF96	227	0.158
SeTl	cP2	221	0.164
$Cd_{33}Na_6$	cP39	200	0.166
$Au_{18}In_{15}Na_6$	cP39	200	0.168
$Cd_{26}Cs_2$	cF112	226	0.173
Ag_2I_2	hP4	186	0.192

for the bulk modulus, tends to provide a slightly worse quantitative agreement but still reproduces trends equally well. The correlations are very high, often above 0.99. Using different values of the Poisson ratio mainly affects Debye temperatures, while having very little effect on Grüneisen parameters. Several different numerical and empirical equations of state have also been investigated. The differences between the results obtained from them are small, but in some cases they are found to introduce an additional source of error compared to a direct evaluation of the bulk modulus from the elastic tensor or from the $E(V)$ curve. Using the different equations of state has very little effect on Debye temperatures, but has more of an effect on Grüneisen parameters. Currently, the values for AGL properties available in the AFLOW repository are those calculated by numerically fitting the $E_{\text{DFT}}(V)$ data and calculating the bulk modulus using Eq. (16). The effect of using different exchange-correlation functionals was investigated for a subset of 16 materials. The results showed that LDA tended to overestimate thermomechanical properties such as bulk modulus or Debye temperature, compared to GGA's tendency to underestimate. However, neither functional was consistently better than the other at predicting trends. We therefore use GGA-PBE for the automated AEL-AGL calculations in order to maintain consistency with the rest of the AFLOW data.

The AEL-AGL evaluation of the Debye temperature provides good agreement with experiment, whereas the predictions of the Grüneisen parameter are quite poor. However, since the Grüneisen parameter is slowly varying for materials

TABLE XXIV. Correlations between experimental values and AEL and AGL results for elastic and thermal properties for the entire set of materials.

Property	Pearson (Linear)	Spearman (Rank Order)	RMSrD
κ^{exp} versus κ^{AGL} ($\sigma = 0.25$) [34]	0.880	0.752	1.293
κ^{exp} versus κ^{AGL}	0.928	0.720	2.614
κ^{exp} versus κ^{BM}	0.879	0.735	2.673
κ^{exp} versus κ^{Vinet}	0.912	0.737	2.443
κ^{exp} versus κ^{BCN}	0.933	0.733	2.751

sharing crystal structures, the AEL-AGL methodology provides a reliable screening tool for identifying materials with very high or very low thermal conductivity. The correlations between the experimental values of the thermal conductivity and those calculated with AGL are summarized in Table XXIV. For the entire set of materials examined we find high values of the Pearson correlation between κ^{exp} and κ^{AGL}, ranging from 0.880 to 0.933. It is particularly high, above 0.9, for materials with high symmetry (cubic, hexagonal or rhombohedral) structures, but significantly lower for anisotropic materials. In our previous work on AGL [34], we used an approximated the value of $\sigma = 0.25$ in Eq. (14). Using instead the Poisson ratio calculated in AEL, σ^{AEL}, the overall correlations are improved by about 5%, from 0.880 to 0.928, in the agreement with previous work on metals [147]. The correlations for anisotropic materials, such as the body-centred tetragonal set examined here, improved even more, demonstrating the significance of a direct evaluation of the Poisson ratio. This combined algorithm demonstrates the advantage of an integrated high-throughput materials design framework such as AFLOW, which enables the calculation of interdependent properties within a single automated workflow.

A direct AEL evaluation of the Poisson ratio, instead of assuming a simple approximation, e.g., a Cauchy solid with $\sigma = 0.25$, consistently improves the correlations of the AGL-Debye temperatures with experiments. However, it has very little effect on the values obtained for the Grüneisen parameter. Simple approximations lead to more numerically robust and better system-size scaling calculations, as they avoid the complications inherent in obtaining the elastic tensor. Therefore AGL could also be used on its own for initial rapid screening, with AEL being performed later for potentially interesting materials to increase the accuracy of the results.

With respect to rapid estimation of thermal conductivities, the approximations in the Leibfried-Schlömann formalism miss some of the details affecting the lattice thermal conductivity, such as the suppression of phonon-phonon scattering due to large gaps between the branches of the phonon dispersion [26]. Nevertheless, the high correlations between κ^{exp} and κ^{AGL} found for most of the structure families in this study demonstrate the utility of the AEL-AGL approach as a screening method for large databases of materials where experimental data is lacking or ambiguous. Despite its intrinsic limitations, the synergy presented by the AEL-AGL approach provides the right balance between accuracy and complexity in identifying materials with promising properties for further investigation.

ACKNOWLEDGMENTS

We thank Drs. Kristin Persson, Gerbrand Ceder, Geoffory Hautier, Anubhav Jain, Shyue Ping Ong, Wei Chen, Patrick Huck, Kiran Mathew, Joseph Montoya, and Donald Winston for various technical discussions. We acknowledge support by the DOE (DE-AC02-05CH11231), specifically the Basic Energy Sciences program under Grant No. EDCBEE. C.T., M.F., M.B.N. and S.C. acknowledge partial support by DOD-ONR (N00014-13-1-0635, N00014-11-1-0136, N00014-15-1-2863). M.B.N. acknowledges the Texas Advanced Computing Center (TACC) at the University of Texas Austin for providing HPC resources. The consortium aflow.org acknowledges Duke University—Center for Materials Genomics—for computational support.

APPENDIX: AFLOW AEL-AGL REST-API

The AEL-AGL methodology described in this work is being used to calculate the elastic and thermal properties of materials in a high-throughput fashion by the AFLOW consortium. The results are now available on the AFLOW database [35,146] via the AFLOW REST-API [36]. The following optional materials keywords have now been added to the AFLOW REST-API to facilitate accessing these data.

(1) `ael_bulk_modulus_reuss`
  (a) *Description.* Returns AEL bulk modulus as calculated using the Reuss average.
  (b) *Type.* `number`.
  (c) *Units.* GPa.
  (d) *Example.* `ael_bulk_modulus_reuss=105.315`.
  (e) *Request syntax.* `$aurl/?ael_bulk_modulus_reuss`.

(2) `ael_bulk_modulus_voigt`
  (a) *Description.* Returns AEL bulk modulus as calculated using the Voigt average.
  (b) *Type.* `number`.
  (c) *Units.* GPa.
  (d) *Example.* `ael_bulk_modulus_voigt=105.315`.
  (e) *Request syntax.* `$aurl/?ael_bulk_modulus_voigt`.

(3) `ael_bulk_modulus_vrh`
  (a) *Description.* Returns AEL bulk modulus as calculated using the Voigt-Reuss-Hill (VRH) average.
  (b) *Type.* `number`.
  (c) *Units.* GPa.
  (d) *Example.* `ael_bulk_modulus_vrh=105.315`.
  (e) *Request syntax.* `$aurl/?ael_bulk_modulus_vrh`.

(4) `ael_elastic_anisotropy`
  (a) *Description.* Returns AEL elastic anisotropy.
  (b) *Type.* `number`.
  (c) *Units.* dimensionless.
  (d) *Example.* `ael_elastic_anisotropy=0.000816153`.
  (e) *Request syntax.* `$aurl/?ael_elastic_anisotropy`.

(5) `ael_poisson_ratio`
  (a) *Description.* Returns AEL Poisson ratio.
  (b) *Type.* `number`.
  (c) *Units.* dimensionless.

(d) *Example.* `ael_elastic_anisotropy`.
(e) *Request syntax.* `$aurl/?ael_poisson_ratio`.

(6) `ael_shear_modulus_reuss`
(a) *Description.* Returns AEL shear modulus as calculated using the Reuss average.
(b) *Type.* `number`.
(c) *Units.* GPa.
(d) *Example.* `ael_shear_modulus_reuss=73.7868`.
(e) *Request syntax.* `$aurl/?ael_shear_modulus_reuss`.

(7) `ael_shear_modulus_voigt`
(a) *Description.* Returns AEL shear modulus as calculated using the Voigt average.
(b) *Type.* `number`.
(c) *Units.* GPa.
(d) *Example.* `ael_shear_modulus_voigt=73.7989`.
(e) *Request syntax.* `$aurl/?ael_shear_modulus_voigt`.

(8) `ael_shear_modulus_vrh`
(a) *Description.* Returns AEL shear modulus as calculated using the Voigt-Reuss-Hill (VRH) average.
(b) *Type.* `number`.
(c) *Units.* GPa.
(d) *Example.* `ael_shear_modulus_vrh=73.7929`.
(e) *Request syntax.* `$aurl/?ael_shear_modulus_vrh`.

(9) `ael_speed_of_sound_average`
(a) *Description.* Returns AEL average speed of sound calculated from the transverse and longitudinal speeds of sound.
(b) *Type.* `number`.
(c) *Units.* $\mathrm{m\,s^{-1}}$.
(d) *Example.* `ael_speed_of_sound_average=500.0`.
(e) *Request syntax.* `$aurl/?ael_speed_of_sound_average`.

(10) `ael_speed_of_sound_longitudinal`
(a) *Description.* Returns AEL speed of sound in the longitudinal direction.
(b) *Type.* `number`.
(c) *Units.* $\mathrm{m\,s^{-1}}$.
(d) *Example.* `ael_speed_of_sound_longitudinal=500.0`.
(e) *Request syntax.* `$aurl/?ael_speed_of_sound_longitudinal`.

(11) `ael_speed_of_sound_transverse`
(a) *Description.* Returns AEL speed of sound in the transverse direction.
(b) *Type.* `number`.
(c) *Units.* $\mathrm{m\,s^{-1}}$.
(d) *Example.* `ael_speed_of_sound_transverse=500.0`.
(e) *Request syntax.* `$aurl/?ael_speed_of_sound_transverse`.

(12) `agl_acoustic_debye`
(a) *Description.* Returns AGL acoustic Debye temperature.
(b) *Type.* `number`.
(c) *Units.* Kelvin.
(d) *Example.* `agl_acoustic_debye=492`.
(e) *Request syntax.* `$aurl/?agl_acoustic_debye`.

(13) `agl_bulk_modulus_isothermal_300K`
(a) *Description.* Returns AGL isothermal bulk modulus at 300 K and zero pressure.
(b) *Type.* `number`.
(c) *Units.* GPa.
(d) *Example.* `agl_bulk_modulus_isothermal_300K=96.6`.
(e) *Request syntax.* `$aurl/?agl_bulk_modulus_isothermal_300K`.

(14) `agl_bulk_modulus_static_300K`
(a) *Description.* Returns AGL static bulk modulus at 300 K and zero pressure.
(b) *Type.* `number`.
(c) *Units.* GPa.
(d) *Example.* `agl_bulk_modulus_static_300K=99.59`.
(e) *Request syntax.* `$aurl/?agl_bulk_modulus_static_300K`.

(15) `agl_debye`
(a) *Description.* Returns AGL Debye temperature.
(b) *Type.* `number`.
(c) *Units.* Kelvin.
(d) *Example.* `agl_debye=620`.
(e) *Request syntax.* `$aurl/?agl_debye`.

(16) `agl_gruneisen`
(a) *Description.* Returns AGL Grüneisen parameter.
(b) *Type.* `number`.
(c) *Units.* dimensionless.
(d) *Example.* `agl_gruneisen=2.06`.
(e) *Request syntax.* `$aurl/?agl_gruneisen`.

(17) `agl_heat_capacity_Cv_300K`
(a) *Description.* Returns AGL heat capacity at constant volume (C_V) at 300 K and zero pressure.
(b) *Type.* `number`.
(c) *Units.* k_B per cell.
(d) *Example.* `agl_heat_capacity_Cv_300K=4.901`.
(e) *Request syntax.* `$aurl/?agl_heat_capacity_Cv_300K`.

(18) `agl_heat_capacity_Cp_300K`
(a) *Description.* Returns AGL heat capacity at constant pressure (C_p) at 300 K and zero pressure.
(b) *Type.* `number`.
(c) *Units.* k_B per cell.
(d) *Example.* `agl_heat_capacity_Cp_300K=5.502`.
(e) *Request syntax.* `$aurl/?agl_heat_capacity_Cp_300K`.

(19) `agl_poisson_ratio_source`
(a) *Description.* Returns source of Poisson ratio used to calculate Debye temperature in AGL. Possible sources include `ael_poisson_ratio_`⟨`value`⟩, in which case the Poisson ratio was calculated from first principles using AEL; `empirical_ratio_`⟨`value`⟩, in which case the value was taken from the literature; and `Cauchy_ratio_0.25`, in which case the default value of 0.25 of the Poisson ratio of a Cauchy solid was used.
(b) *Type.* `string`.

(c) *Example.* `agl_poisson_ratio_source=ael_poisson_ratio_0.193802`.

(d) *Request syntax.* `$aurl/?agl_poisson_ratio_source`.

(20) `agl_thermal_conductivity_300K`

(a) *Description.* Returns AGL thermal conductivity at 300K.

(b) *Type.* `number`.

(c) *Units.* $\mathrm{W\,m^{-1}\,K^{-1}}$.

(d) *Example.* `agl_thermal_conductivity_300K=24.41`.

(e) *Request syntax.* `$aurl/?agl_thermal_conductivity_300K`.

(21) `agl_thermal_expansion_300K`

(a) *Description.* Returns AGL thermal expansion at 300K and zero pressure.

(b) *Type.* `number`.

(c) *Units.* $\mathrm{K^{-1}}$.

(d) *Example.* `agl_thermal_expansion_300K=4.997e-05`.

(e) *Request syntax.* `$aurl/?agl_thermal_expansion_300K`.

[1] G. N. Greaves, A. L. Greer, R. S. Lakes, and T. Rouxel, Poisson's ratio and modern materials, Nat. Mater. **10**, 823 (2011).

[2] J.-P. Poirier, *Introduction to the Physics of the Earth's Interior*, 2nd ed. (Cambridge University Press, Cambridge, 2000).

[3] F. Mouhat and F.-X. Coudert, Necessary and sufficient elastic stability conditions in various crystal systems, Phys. Rev. B **90**, 224104 (2014).

[4] S. Barzilai, C. Toher, S. Curtarolo, and O. Levy, Evaluation of the tantalum-titanium phase diagram from *ab-initio* calculations, Acta Mater. **120**, 255 (2016).

[5] X. Q. Chen, H. Niu, D. Li, and Y. Li, Modeling hardness of polycrystalline materials and bulk metallic glasses, Intermetallics **19**, 1275 (2011).

[6] M. Zebarjadi, K. Esfarjani, M. S. Dresselhaus, Z. F. Ren, and G. Chen, Perspectives on thermoelectrics: From fundamentals to device applications, Energy Environ. Sci. **5**, 5147 (2012).

[7] J. Carrete, W. Li, N. Mingo, S. Wang, and S. Curtarolo, Finding Unprecedentedly Low-Thermal-Conductivity Half-Heusler Semiconductors via High-Throughput Materials Modeling, Phys. Rev. X **4**, 011019 (2014).

[8] K. F. Garrity, First-principles search for *n*-type oxide, nitride, and sulfide thermoelectrics, Phys. Rev. B **94**, 045122 (2016).

[9] K. Watari and S. L. Shinde, High thermal conductivity materials, MRS Bull. **26**, 440 (2001).

[10] L.-T. Yeh and R. C. Chu, *Thermal Management of Microloectronic Equipment: Heat Transfer Theory, Analysis Methods, and Design Practices* (ASME Press, New York, 2002).

[11] M. J. Mehl and D. A. Papaconstantopoulos, Applications of a tight-binding total-energy method for transition and noble metals: Elastic constants, vacancies, and surfaces of monatomic metals, Phys. Rev. B **54**, 4519 (1996).

[12] M. J. Mehl, B. M. Klein, and D. A. Papaconstantopolous, First principles calculation of elastic properties, in *Intermetallic Compounds: Principles and Practice*, edited by J. H. Westbrook and R. L. Fleischer (Wiley, New York, 1995).

[13] R. Golesorkhtabar, P. Pavone, J. Spitaler, P. Puschnig, and C. Draxl, ElaStic: A tool for calculating second-order elastic constants from first principles, Comput. Phys. Commun. **184**, 1861 (2013).

[14] M. de Jong, W. Chen, T. Angsten, A. Jain, R. Notestine, A. Gamst, M. Sluiter, C. K. Ande, S. van der Zwaag, J. J. Plata, C. Toher, S. Curtarolo, G. Ceder, K. A. Persson, and M. D. Asta, Charting the complete elastic properties of inorganic crystalline compounds, Sci. Data **2**, 150009 (2015).

[15] P. R. C. da Silveira, C. R. S. da Silva, and R. M. Wentzcovitch, Metadata management for distributed first principles calculations in *VLab*—A collaborative cyberinfrastructure for materials computation, Comput. Phys. Commun. **178**, 186 (2008).

[16] C. R. S. da Silva, P. R. C. da Silveira, B. Karki, R. M. Wentzcovitch, P. A. Jensen, E. F. Bollig, M. Pierce, G. Erlebacher, and D. A. Yuen, Virtual laboratory for planetary materials: System service architecture overview, Phys. Earth Planet. Inter. **163**, 321 (2007).

[17] S. Curtarolo, W. Setyawan, G. L. W. Hart, M. Jahnátek, R. V. Chepulskii, R. H. Taylor, S. Wang, J. Xue, K. Yang, O. Levy, M. J. Mehl, H. T. Stokes, D. O. Demchenko, and D. Morgan, AFLOW: An automatic framework for high-throughput materials discovery, Comput. Mater. Sci. **58**, 218 (2012).

[18] O. Levy, G. L. W. Hart, and S. Curtarolo, Uncovering compounds by synergy of cluster expansion and high-throughput methods, J. Am. Chem. Soc. **132**, 4830 (2010).

[19] G. L. W. Hart, S. Curtarolo, T. B. Massalski, and O. Levy, Comprehensive Search for New Phases and Compounds in Binary Alloy Systems Based on Platinum-Group Metals, Using a Computational First-Principles Approach, Phys. Rev. X **3**, 041035 (2013).

[20] D. A. Broido, M. Malorny, G. Birner, N. Mingo, and D. A. Stewart, Intrinsic lattice thermal conductivity of semiconductors from first principles, Appl. Phys. Lett. **91**, 231922 (2007).

[21] W. Li, N. Mingo, L. Lindsay, D. A. Broido, D. A. Stewart, and N. A. Katcho, Thermal conductivity of diamond nanowires from first principles, Phys. Rev. B **85**, 195436 (2012).

[22] A. Ward, D. A. Broido, D. A. Stewart, and G. Deinzer, *Ab initio* theory of the lattice thermal conductivity in diamond, Phys. Rev. B **80**, 125203 (2009).

[23] A. Ward and D. A. Broido, Intrinsic phonon relaxation times from first-principles studies of the thermal conductivities of Si and Ge, Phys. Rev. B **81**, 085205 (2010).

[24] Q. Zhang, F. Cao, K. Lukas, W. Liu, K. Esfarjani, C. Opeil, D. Broido, D. Parker, D. J. Singh, G. Chen, and Z. Ren, Study of the thermoelectric properties of lead selenide doped with boron, gallium, indium, or thallium, J. Am. Chem. Soc. **134**, 17731 (2012).

[25] W. Li, L. Lindsay, D. A. Broido, D. A. Stewart, and N. Mingo, Thermal conductivity of bulk and nanowire $Mg_2Si_xSn_{1-x}$ alloys from first principles, Phys. Rev. B **86**, 174307 (2012).

[26] L. Lindsay, D. A. Broido, and T. L. Reinecke, First-Principles Determination of Ultrahigh Thermal Conductivity of Boron

Arsenide: A Competitor for Diamond? Phys. Rev. Lett. **111**, 025901 (2013).

[27] L. Lindsay, D. A. Broido, and T. L. Reinecke, *Ab initio* thermal transport in compound semiconductors, Phys. Rev. B **87**, 165201 (2013).

[28] M. S. Green, Markoff random processes and the statistical mechanics of time-dependent phenomena. II. Irreversible processes in fluids, J. Chem. Phys. **22**, 398 (1954).

[29] R. Kubo, Statistical-mechanical theory of irreversible processes. I. General theory and simple applications to magnetic and conduction problems, J. Phys. Soc. Jpn. **12**, 570 (1957).

[30] S. Curtarolo and G. Ceder, Dynamics of an Inhomogeneously Coarse Grained Multiscale System, Phys. Rev. Lett. **88**, 255504 (2002).

[31] S. Curtarolo, G. L. W. Hart, M. Buongiorno Nardelli, N. Mingo, S. Sanvito, and O. Levy, The high-throughput highway to computational materials design, Nat. Mater. **12**, 191 (2013).

[32] M. A. Blanco, E. Francisco, and V. Luaña, GIBBS: isothermal-isobaric thermodynamics of solids from energy curves using a quasi-harmonic Debye model, Comput. Phys. Commun. **158**, 57 (2004).

[33] M. A. Blanco, A. M. Pendás, E. Francisco, J. M. Recio, and R. Franco, Thermodynamical properties of solids from microscopic theory: Applications to MgF_2 and Al_2O_3, J. Mol. Struct., Theochem **368**, 245 (1996).

[34] C. Toher, J. J. Plata, O. Levy, M. de Jong, M. D. Asta, M. Buongiorno Nardelli, and S. Curtarolo, High-throughput computational screening of thermal conductivity, Debye temperature, and Grüneisen parameter using a quasiharmonic Debye model, Phys. Rev. B **90**, 174107 (2014).

[35] S. Curtarolo, W. Setyawan, S. Wang, J. Xue, K. Yang, R. H. Taylor, L. J. Nelson, G. L. W. Hart, S. Sanvito, M. Buongiorno Nardelli, N. Mingo, and O. Levy, AFLOWLIB.ORG: A distributed materials properties repository from high-throughput *ab initio* calculations, Comput. Mater. Sci. **58**, 227 (2012).

[36] R. H. Taylor, F. Rose, C. Toher, O. Levy, K. Yang, M. Buongiorno Nardelli, and S. Curtarolo, A RESTful API for exchanging materials data in the AFLOWLIB.org consortium, Comput. Mater. Sci. **93**, 178 (2014).

[37] C. E. Calderon, J. J. Plata, C. Toher, C. Oses, O. Levy, M. Fornari, A. Natan, M. J. Mehl, G. L. W. Hart, M. Buongiorno Nardelli, and S. Curtarolo, The AFLOW standard for high-throughput materials science calculations, Comput. Mater. Sci. **108**, 233 (2015).

[38] K. Yang, C. Oses, and S. Curtarolo, Modeling off-stoichiometry materials with a high-throughput *ab-initio* approach, Chem. Mater. **28**, 6484 (2016).

[39] A. Jain, G. Hautier, C. J. Moore, S. P. Ong, C. C. Fischer, T. Mueller, K. A. Persson, and G. Ceder, A high-throughput infrastructure for density functional theory calculations, Comput. Mater. Sci. **50**, 2295 (2011).

[40] A. Jain, S. P. Ong, G. Hautier, W. Chen, W. D. Richards, S. Dacek, S. Cholia, D. Gunter, D. Skinner, G. Ceder, and K. A. Persson, Commentary: The materials project: A materials genome approach to accelerating materials innovation, APL Mater. **1**, 011002 (2013).

[41] S. P. Ong, W. D. Richards, A. Jain, G. Hautier, M. Kocher, S. Cholia, D. Gunter, V. L. Chevrier, K. A. Persson, and G. Ceder, Python Materials Genomics (pymatgen): A robust, open-source python library for materials analysis, Comput. Mater. Sci. **68**, 314 (2013).

[42] W. Setyawan and S. Curtarolo, High-throughput electronic band structure calculations: Challenges and tools, Comput. Mater. Sci. **49**, 299 (2010).

[43] O. Levy, R. V. Chepulskii, G. L. W. Hart, and S. Curtarolo, The new face of rhodium alloys: Revealing ordered structures from first principles, J. Am. Chem. Soc. **132**, 833 (2010).

[44] O. Levy, G. L. W. Hart, and S. Curtarolo, Structure maps for hcp metals from first-principles calculations, Phys. Rev. B **81**, 174106 (2010).

[45] O. Levy, M. Jahnátek, R. V. Chepulskii, G. L. W. Hart, and S. Curtarolo, Ordered structures in rhenium binary alloys from first-principles calculations, J. Am. Chem. Soc. **133**, 158 (2011).

[46] M. Jahnátek, O. Levy, G. L. W. Hart, L. J. Nelson, R. V. Chepulskii, J. Xue, and S. Curtarolo, Ordered phases in ruthenium binary alloys from high-throughput first-principles calculations, Phys. Rev. B **84**, 214110 (2011).

[47] R. H. Taylor, S. Curtarolo, and G. L. W. Hart, Guiding the experimental discovery of magnesium alloys, Phys. Rev. B **84**, 084101 (2011).

[48] R. Hill, The elastic behavior of a crystalline aggregate, Proc. Phys. Soc. Sect. A **65**, 349 (1952).

[49] F. Birch, The effect of pressure upon the elastic parameters of isotropic solids, according to Murnaghan's theory of finite strain, J. Appl. Phys. **9**, 279 (1938).

[50] P. Vinet, J. H. Rose, J. Ferrante, and J. R. Smith, Universal features of the equation of state of solids, J. Phys.: Condens. Matter **1**, 1941 (1989).

[51] V. G. Baonza, M. Cáceres, and J. Núñez, Universal compressibility behavior of dense phases, Phys. Rev. B **51**, 28 (1995).

[52] G. Leibfried and E. Schlömann, *Wärmeleitung in elektrisch isolierenden Kristallen*, Nachrichten d. Akad. d. Wiss. in Göttingen. Math.-physik. Kl. 2a. Math.-physik.-chem. Abt (Vandenhoeck and Ruprecht, Göttingen, Germany, 1954).

[53] G. A. Slack, *The Thermal Conductivity of Nonmetallic Crystals*, edited by H. Ehrenreich, F. Seitz, and D. Turnbull, Solid State Physics Vol. 34 (Academic, New York, 1979), p. 1.

[54] D. T. Morelli and G. A. Slack, High lattice thermal conductivity solids, in *High Thermal Conductivity Materials*, edited by S. L. Shindé and J. S. Goela (Springer, New York, 2006).

[55] L. Bjerg, B. B. Iversen, and G. K. H. Madsen, Modeling the thermal conductivities of the zinc antimonides ZnSb and Zn_4Sb_3, Phys. Rev. B **89**, 024304 (2014).

[56] P. Nath, J. J. Plata, D. Usanmaz, R. Al Rahal Al Orabi, M. Fornari, M. Buongiorno Nardelli, C. Toher, and S. Curtarolo, High-throughput prediction of finite-temperature properties using the quasi-harmonic approximation, Comput. Mater. Sci. **125**, 82 (2016).

[57] D. Wee, B. Kozinsky, B. Pavan, and M. Fornari, Quasiharmonic vibrational properties of TiNiSn from *ab-initio* phonons, J. Electron. Mater. **41**, 977 (2012).

[58] P. Nath, J. J. Plata, D. Usanmaz, C. Toher, M. Fornari, M. Buongiorno Nardelli, and S. Curtarolo, High throughput combinatorial method for fast and robust prediction of lattice thermal conductivity, Scr. Mater. **129**, 88 (2017).

[59] G. Kresse and J. Hafner, *Ab initio* molecular dynamics for liquid metals, Phys. Rev. B **47**, 558 (1993).

[60] P. E. Blöchl, Projector augmented-wave method, Phys. Rev. B **50**, 17953 (1994).
[61] J. P. Perdew, K. Burke, and M. Ernzerhof, Generalized Gradient Approximation Made Simple, Phys. Rev. Lett. **77**, 3865 (1996).
[62] M. J. Mehl, D. Hicks, C. Toher, O. Levy, R. M. Hanson, G. L. W. Hart, and S. Curtarolo, The AFLOW library of crystallographic prototypes, Comput. Mater. Sci. (2017), doi:10.1016/j.commatsci.2017.01.017.
[63] http://aflow.org/CrystalDatabase/AB_cF8_216_c_a.html
[64] http://aflow.org/CrystalDatabase/A_cF8_227_a.html
[65] See Supplemental Material at http://link.aps.org/supplemental/10.1103/PhysRevMaterials.1.015401 for tables of thermal property values calculated with different equations of state, tables of calculated and experimental elastic constants, and tables with AFLOW unique identifiers (AUIDs) for highest and lowest thermal conductivity materials in AFLOW database.
[66] O. Madelung (ed.), *Semiconductors - Basic Data*, 2nd ed. (Springer, Berlin, 1996).
[67] P. K. Lam, M. L. Cohen, and G. Martinez, Analytic relation between bulk moduli and lattice constants, Phys. Rev. B **35**, 9190 (1987).
[68] M. H. Grimsditch and A. K. Ramdas, Brillouin scattering in diamond, Phys. Rev. B **11**, 3139 (1975).
[69] K. Strössner, M. Cardona, and W. J. Choyke, High pressure X-ray investigations on 3C-SiC, Solid State Commun. **63**, 113 (1987).
[70] W. A. Fate, High-temperature shear modulus of Si_3N_4 and SiC, J. Am. Ceram. Soc. **57**, 49 (1974).
[71] J. J. Hall, Electronic effects in the elastic constants of *n*-type silicon, Phys. Rev. **161**, 756 (1967).
[72] L. J. Bruner and R. W. Keyes, Electronic Effect in the Elastic Constants of Germanium, Phys. Rev. Lett. **7**, 55 (1961).
[73] W. Wettling and J. Windscheif, Elastic constants and refractive index of boron phosphide, Solid State Commun. **50**, 33 (1984).
[74] T. Suzuki, T. Yagi, S. Akimoto, T. Kawamura, S. Toyoda, and S. Endo, Compression behavior of CdS and BP up to 68 GPa, J. Appl. Phys. **54**, 748 (1983).
[75] R. G. Greene, H. Luo, T. Li, and A. L. Ruoff, Phase Transformation of AlAs to NiAs Structure at High Pressure, Phys. Rev. Lett. **72**, 2045 (1994).
[76] D. I. Bolef and M. Menes, Elastic constants of single-crystal aluminum antimonide, J. Appl. Phys. **31**, 1426 (1960).
[77] R. Weil, Correction to the elastic constants of AlSb, J. Appl. Phys. **43**, 4271 (1972).
[78] W. F. Boyle and R. J. Sladek, Elastic constants and lattice anharmonicity of GaSb and GaP from ultrasonic-velocity measurements between 4.2 and 300 K, Phys. Rev. B **11**, 2933 (1975).
[79] T. B. Bateman, H. J. McSkimin, and J. M. Whelan, Elastic moduli of single-crystal gallium arsenide, J. Appl. Phys. **30**, 544 (1959).
[80] D. N. Nichols, D. S. Rimai, and R. J. Sladek, Elastic anharmonicity of InP: Its relationship to the high pressure transition, Solid State Commun. **36**, 667 (1980).
[81] D. Gerlich, Elastic constants of single-crystal indium arsenide, J. Appl. Phys. **34**, 2915 (1963).
[82] L. H. DeVaux and F. A. Pizzarello, Elastic constants of indium antimonide, Phys. Rev. **102**, 85 (1956).
[83] L. J. Slutsky and C. W. Garland, Elastic constants of indium antimonide from 4.2°K to 300°K, Phys. Rev. **113**, 167 (1959).
[84] C. A. Vanderborgh, Y. K. Vohra, and A. L. Ruoff, Structural phase transitions in InSb to 66 GPa, Phys. Rev. B **40**, 12450 (1989).
[85] B. H. Lee, Elastic constants of ZnTe and ZnSe between 77°–300°K, J. Appl. Phys. **41**, 2984 (1970).
[86] A. Lehoczky, D. A. Nelson, and C. R. Whitsett, Elastic constants of mercury selenide, Phys. Rev. **188**, 1069 (1969).
[87] R. I. Cottam and G. A. Saunders, The elastic behavior of mercury telluride, J. Phys. Chem. Solids **36**, 187 (1975).
[88] E. S. Toberer, A. Zevalkink, and G. J. Snyder, Phonon engineering through crystal chemistry, J. Mater. Chem. **21**, 15843 (2011).
[89] Ioffe Physico - Technical Institute, http://www.ioffe.ru/SVA/NSM/Semicond/index.html
[90] Springer Materials: The Landolt-Börnstein Database, http://materials.springer.com
[91] D. P. Spitzer, Lattice thermal conductivity of semiconductors: A chemical bond approach, J. Phys. Chem. Solids **31**, 19 (1970).
[92] C. R. Whitsett, D. A. Nelson, J. G. Broerman, and E. C. Paxhia, Lattice thermal conductivity of mercury selenide, Phys. Rev. B **7**, 4625 (1973).
[93] http://aflow.org/CrystalDatabase/AB_cF8_225_a_b.html
[94] D. Laplaze, M. Boissier, and R. Vacher, Velocity of hypersounds in lithium hydride by spontaneous Brillouin scattering, Solid State Commun. **19**, 445 (1976).
[95] S. Haussühl, Thermo-elastische Konstanten der Alkalihalogenide vom NaCl-Typ, Z. Phys. **159**, 223 (1960).
[96] W. C. Hughes and L. S. Cain, Second-order elastic constants of AgCl from 20 to 430 °C, Phys. Rev. B **53**, 5174 (1996).
[97] Y. Sumino, I. Ohno, T. Goto, and M. Kumazawa, Measurement of elastic constants and internal frictions on single-crystal MgO by rectangular parallelepiped resonance, J. Phys. Earth **24**, 263 (1976).
[98] Z. P. Chang and E. K. Graham, Elastic properties of oxides in the NaCl-structure, J. Phys. Chem. Solids **38**, 1355 (1977).
[99] G. I. Peresada, E. G. Ponyatovskii, and Z. D. Sokolovskaya, Pressure dependence of the elastic constants of PbS, Phys. Stat. Solidi A **35**, K177 (1976).
[100] G. Lippmann, P. Kästner, and W. Wanninger, Elastic constants of PbSe, Phys. Stat. Solidi A **6**, K159 (1971).
[101] A. J. Miller, G. A. Saunders, and Y. K. Yogurtcu, Pressure dependences of the elastic constants of PbTe, SnTe and $Ge_{0.08}Sn_{0.92}Te$, J. Phys. C **14**, 1569 (1981).
[102] T. Seddon, S. C. Gupta, and G. A. Saunders, Hole contribution to the elastic constants of SnTe, Solid State Commun. **20**, 69 (1976).
[103] M. Anis-ur-Rehman and A. Maqsood, Measurement of thermal transport properties with an improved transient plane source technique, Int. J. Thermophys. **24**, 867 (2003).
[104] http://aflow.org/CrystalDatabase/AB_hP4_186_b_b.html
[105] G. Arlt and G. R. Schodder, Some elastic constants of silicon carbide, J. Acoust. Soc. Am. **37**, 384 (1965).
[106] L. E. McNeil, M. Grimsditch, and R. H. French, Vibrational spectroscopy of aluminum nitride, J. Am. Ceram. Soc. **76**, 1132 (1993).
[107] S. P. Dodd, G. A. Saunders, M. Cankurtaran, and B. James, Ultrasonic study of the elastic and nonlinear acoustic properties of ceramic aluminum nitride, J. Mater. Sci. **36**, 723 (2001).

[108] V. A. Savastenko and A. U. Sheleg, Study of the elastic properties of gallium nitride, Phys. Stat. Solidi A **48**, K135 (1978).
[109] A. Polian, M. Grimsditch, and I. Grzegory, Elastic constants of gallium nitride, J. Appl. Phys. **79**, 3343 (1996).
[110] I. B. Kobiakov, Elastic, piezoelectric and dielectric properties of ZnO and CdS single crystals in a wide range of temperatures, Solid State Commun. **35**, 305 (1980).
[111] C. F. Cline, H. L. Dunegan, and G. W. Henderson, Elastic constants of hexagonal BeO, ZnS, and CdSe, J. Appl. Phys. **38**, 1944 (1967).
[112] M. Gatulle, M. Fischer, and A. Chevy, Elastic constants of the layered compounds GaS, GaSe, InSe, and their pressure dependence I. Experimental part, Phys. Stat. Solidi B **119**, 327 (1983).
[113] M. Ueno, M. Yoshida, A. Onodera, O. Shimomura, and K. Takemura, Stability of the wurtzite-type structure under high pressure: GaN and InN, Phys. Rev. B **49**, 14 (1994).
[114] S. Krukowski, A. Witek, J. Adamczyk, J. Jun, M. Bockowski, I. Grzegory, B. Lucznik, G. Nowak, M. Wróblewski, A. Presz, S. Gierlotka, S. Stelmach, B. Palosz, S. Porowski, and P. Zinn, Thermal properties of indium nitride, J. Phys. Chem. Solids **59**, 289 (1998).
[115] G. A. Slack and S. F. Bartram, Thermal expansion of some diamond-like crystals, J. Appl. Phys. **46**, 89 (1975).
[116] http://aflow.org/CrystalDatabase/A2B3_hR5_166_c_ac.html
[117] http://aflow.org/CrystalDatabase/A2B3_hR10_167_c_e.html
[118] J. O. Jenkins, J. A. Rayne, and R. W. Ure, Jr., Elastic moduli and phonon properties of Bi_2Te_3, Phys. Rev. B **5**, 3171 (1972).
[119] T. Goto, O. L. Anderson, I. Ohno, and S. Yamamoto, Elastic constants of corundum up to 1825 K, J. Geophys. Res. Solid Earth **94**, 7588 (1989).
[120] H. L. Alberts and J. C. A. Boeyens, The elastic constants and distance dependence of the magnetic interactions of Cr_2O_3, J. Magn. Magn. Mater. **2**, 327 (1976).
[121] G. A. Slack, Thermal conductivity of MgO, Al_2O_3, $MgAl_2O_4$, and Fe_3O_4 crystals from 3° to 300°K, Phys. Rev. **126**, 427 (1962).
[122] R. H. Bruce and D. S. Cannell, Specific heat of Cr_2O_3 near the Néel temperature, Phys. Rev. B **15**, 4451 (1977).
[123] http://aflow.org/CrystalDatabase/ABC2_tI16_122_a_b_d.html
[124] B. Fernández and S. M. Wasim, Sound velocities and elastic moduli in $CuInTe_2$ and $CuInSe_2$, Phys. Stat. Solidi A **122**, 235 (1990).
[125] H. Neumann, Bulk modulus-volume relationship in ternary chalcopyrite compounds, Phys. Stat. Solidi A **96**, K121 (1986).
[126] M. H. Grimsditch and G. D. Holah, Brillouin scattering and elastic moduli of silver thiogallate ($AgGaS_2$), Phys. Rev. B **12**, 4377 (1975).
[127] T. Hailing, G. A. Saunders, W. A. Lambson, and R. S. Feigelson, Elastic behavior of the chalcopyrite $CdGeAs_2$, J. Phys. C **15**, 1399 (1982).
[128] M. Bettini and W. B. Holzapfel, Grüneisen parameters of Γ phonons in $CdSiP_2$, $CuAlS_2$, and $CuGaS_2$, Solid State Commun. **16**, 27 (1975).
[129] J. D. Beasley, Thermal conductivities of some novel nonlinear optical materials, Appl. Opt. **33**, 1000 (1994).
[130] S. C. Abrahams and F. S. L. Hsu, Debye temperatures and cohesive properties, J. Chem. Phys. **63**, 1162 (1975).
[131] J. L. Shay and J. H. Wernick, *Ternary Chalcopyrite Semiconductors: Growth, Electronic Properties, and Applications* (Pergamon, Oxford, UK, 1975).
[132] K. Masumoto, S. Isomura, and W. Goto, The preparation and properties of $ZnSiAs_2$, $ZnGeP_2$, and $CdGeP_2$ semiconducting compounds, J. Phys. Chem. Solids **27**, 1939 (1966).
[133] K. Bohmhammel, P. Deus, and H. A. Schneider, Specific heat, Debye temperature, and related properties of compound semiconductors $A^{II}B^{IV}C_2^V$, Phys. Stat. Solidi A **65**, 563 (1981).
[134] C. Rincón, M. L. Valeri-Gil, and S. M. Wasim, Room-temperature thermal conductivity and Grüneisen parameter of the I–III–VI_2 chalcopyrite compounds, Phys. Stat. Solidi A **147**, 409 (1995).
[135] K. Bohmhammel, P. Deus, G. Kühn, and W. Möller, Specific heat, Debye temperature, and related properties of chalcopyrite semiconducting compounds $CuGaSe_2$, $CuGaTe_2$, and $CuInTe_2$, Phys. Status Solidi A **71**, 505 (1982).
[136] http://aflow.org/CrystalDatabase/A3B_cI32_204_g_c.html
[137] http://aflow.org/CrystalDatabase/AB_oP16_61_c_c.html
[138] http://aflow.org/CrystalDatabase/AB_cP2_221_b_a.html
[139] http://aflow.org/CrystalDatabase/A2B_tP6_136_f_a.html
[140] T. Chattopadhyay, R. P. Santandrea, and H. G. von Schnering, Temperature and pressure dependence of the crystal structure of InTe: A new high pressure phase of InTe, J. Phys. Chem. Solids **46**, 351 (1985).
[141] E. Chang and E. K. Graham, The elastic constants of cassiterite SnO_2 and their pressure and temperature dependence, J. Geophys. Res. **80**, 2595 (1975).
[142] P. H. M. Böttger, K. Valset, S. Deledda, and T. G. Finstad, Influence of ball-milling, nanostructuring, and Ag inclusions on thermoelectric properties of ZnSb, J. Electron. Mater. **39**, 1583 (2010).
[143] P. Türkes, C. Pluntke, and R. Helbig, Thermal conductivity of SnO_2 single crystals, J. Phys. C **13**, 4941 (1980).
[144] L. He, F. Liu, G. Hautier, M. J. T. Oliveira, M. A. L. Marques, F. D. Vila, J. J. Rehr, G.-M. Rignanese, and A. Zhou, Accuracy of generalized gradient approximation functionals for density-functional perturbation theory calculations, Phys. Rev. B **89**, 064305 (2014).
[145] F. Saadaoui, F. Z. D. Khodja, A.-E.-D. Kadoun, M. D. Khodja, A. Elias, and A. Boudali, First-principles calculations of structural, elastic, thermodynamic, and electronic properties of anti-perovskites $A^{III}CNi_3$ (A^{III} = Al, Ga, In), Eur. Phys. J. D **88**, 316 (2015).
[146] AflowLib: Ab-initio Electronic Structure Library Database, http://www.aflow.org (2011).
[147] X. L. Liu, B. K. VanLeeuwen, S.-L. Shang, Y. Du, and Z.-K. Liu, On the scaling factor in Debye-Grüneisen model: A case study of the Mg-Zn binary system, Comput. Mater. Sci. **98**, 34 (2015).